

Report to Division of Forestry, Fire, and State Lands, 05-20-11

**Spatial variation of mercury methylation in Farmington and Ogden Bays,
Great Salt Lake, UT: correlation to organic matter content in sediment**

William P. Johnson*, Abigail Rudd

Diego P. Fernandez, Gregory T. Carling,

Dept. of Geology & Geophysics

University of Utah, Salt Lake City, UT 84112

Executive Summary

In order to consider means to mitigate methylation of mercury in large systems such as the Great Salt Lake, it is necessary to identify areas where mercury is being produced. The spatial variability of methyl mercury production in freshwater-influenced bays of the Great Salt Lake was examined via collection of sediment and water samples from multiple sites on multiple transects at the north and south ends of Farmington Bay in summer and fall, 2009, and the north end of Ogden Bay in summer 2010. Subsamples were spiked with $^{204}\text{Hg}^{2+}$ to examine net production of methyl ^{204}Hg over time. Isotope-specific mercury concentrations in the incubated sub-samples were detected using cold vapor atomic fluorescence spectrometry in line with inductively couple plasma mass

* Corresponding author. Email: william.johnson@utah.edu. Tel: (801)585-5033. Fax: (801)581-7065.

spectrometry. First order methylation rate constants (k_{meth}) for each site were backed out from the observed changes in isotope ratio as a function of incubation time. As expected, methylation was not significant in overlying water samples, but was significant in sediment samples, and k_{meth} showed spatial variation that did not correspond to methyl or total Hg concentrations, water column salinity or dissolved oxygen. However, a positive correlation with between K_{meth} and sediment organic carbon content was observed, indicating increased methylation potential in sediments with higher organic carbon content. The study indicates that it may be possible to identify areas of higher methyl mercury production based on the amount of organic matter in the sediment, the latter being a simple and cheap analysis.

Introduction

Many recent studies have examined the relationship between methyl mercury (MeHg) concentrations and other parameters in aquatic sediments in order to understand what parameters measured in field studies most closely reflect the dynamic processes controlling mercury production and accumulation. Some previous studies suggest a direct relationship between MeHg and THg in both water and sediment phases (1, 2, 3). Some studies observe direct correlation of sediment MeHg and sediment organic carbon concentrations (3, 4, 5), which can potentially be expected on the basis that sediment organic matter drives heterotrophic bacterial activity that consumes oxygen and drives iron and sulfate reduction that yields mercury methylation. However, in cases where no such relationship is discerned, it is likely that this relationship is obscured by transport of

MeHg from sediment pore water to the water column (6), as well as by demethylation of MeHg. Mercury methylation and demethylation are dynamic processes that control MeHg concentration. Whereas mechanistic studies have examined the role of sulfate, sulfide, organic matter, and other parameters on methylation in sediment, the relationship of these parameters to methylation rate and MeHg concentration and at the field scale seems to be site-specific. Some studies have observed a positive correlation between mercury methylation rates and sediment organic matter content (4, 5). Some studies show that methylation rate and MeHg concentration are uncorrelated for sediments underlying brackish surface water (7), but are correlated in freshwater sediment (5, 7) as well as near-shore marine sediment (2, 6, 8). Rolfhus *et al.* (9), proposed that increased salinity may enhance the formation of reactive Hg thereby making Hg more readily available for methylation, suggesting that methylation and salinity may be positively correlated.

The Great Salt Lake (GSL), a terminal lake located in northwestern Utah, is an important ecosystem for millions of migratory birds and is a site of hemispheric importance recognized by the Western Hemisphere Shorebird Reserve Network (10), with over 1.4 million shorebirds using the GSL and surrounding wetlands for breeding and staging areas (11). Three species of waterfowl currently have consumption advisories issued by the Utah Department of Health due to mercury levels that exceed the EPA screening value (0.3 mg/kg) measured in the muscle tissue of these ducks (12), and other species

nesting on GSL (California gulls and Eared grebes) also have elevated mercury concentrations in their blood (13, 14).

The deep brine layer of GSL contains among the highest concentrations of methyl mercury measured by the USGS Mercury Research Laboratory (15). The deep brine layer is one component of a system of vertically and horizontally connected “compartments”, including shallow and deep brine layers in the main bays, e.g. Gilbert Bay (Figure 1), as well as bays on the eastern side (Bear River, Ogden, and Farmington) where fresh water is delivered from the corresponding rivers (Bear, Weber, and Jordan, respectively) (Figure 1), and where metropolitan effluent from the majority of Utah’s population, about 2 million people, is received. The deep brine layer is anoxic as well as rich in organic carbon (16), and results from pooling of higher salinity (higher density) water that flows from Gunnison Bay into Gilbert Bay. Density stratification also occurs to some extent (and ephemerally) in Farmington and Bear River Bays due to wind- or stage-driven flow of saline water from Gilbert Bay into these relatively freshwater bays, for example through the causeway at site FBN-3 in Figure 1.

This study investigates spatial distribution of total and methyl mercury and methylation potentials in sediment and water samples from four transects in Farmington and Ogden Bays, GSL, Utah (Figure 1). Methylation potential was assessed via spiking of microcosm samples with $^{204}\text{Hg}^{2+}$ to serve as an isotopic tracer. Methylation rates were obtained from kinetic modeling of the observed change in isotopic ratios over time. The

methylation rates were compared total (THg) and MeHg concentrations, salinity, organic carbon content of sediment, and other parameters to determine those parameters that may reflect the spatial variation of mercury methylation in these bays.

Materials and Methods

Field

Sediment and water column samples were taken at four to five sites along two east-west trending transects at the north and south ends of Farmington Bay, and a transect at the north end of Ogden Bay (Figure 1). Sampling of the Farmington Bay transects was performed during summer (July 13th and August 18th) and fall (November 11th and September 28th), 2009. Sampling of the Ogden Bay transect was performed during summer (August 12th) 2010. Water depths measured at the south transect of Farmington Bay (FBS), near the major inlet source (Jordan River) were much shallower (≤ 10 cm) relative to the north transect (FBN), which spans the outlet into Ogden Bay. Maximum water depths of one meter were observed for the three westernmost sites of FBN (located near the outlet) with decreasing water column depth to the east. Water depths at the Ogden Bay transect (OB) were similar to those at FBS (< 20 cm depth). Sites were accessed by raft, air boat and hovercraft.



Figure 1. Location map of the transects and sampling sites in Farmington Bay (FBN and FBS) and Ogden Bay (OB), Great Salt Lake, Utah.

Water quality parameters (T, pH, DO, and conductivity) as well as sulfide and major anions (F^- , Cl^- , NO_3^- , SO_4^{2-}) were measured as described in the [Supporting Information](#). Dissolved organic carbon analyses were performed from water samples from two of the transects (FBN summer and FBS summer), as described in the [Supporting Information](#).

Sediment cores (20-30 cm) were collected using cellulose acetate butyrate (CAB) tubing pushed vertically into sediment underlying the water column. The exposed tube end was capped and sealed with electrical tape, and the tube was lifted vertically, gently, and quickly to retain the sediment and overlying water. The bottom of the tube was capped under water, and sealed with electrical tape. Once on board the craft, the top end of the tube was cut (via a scoring tube cutter), and drained to about 5-6 cm above the sediment surface (where water column measurements indicated overlying water was anoxic), and was recapped (releasing any headspace air via pressing the cap), and sealed with electrical tape. On shore, the sealed sediment cores with overlying water were placed vertically into N₂-pressured containers and stored on ice in coolers.

Laboratory

For spiked sub-samples, ²⁰⁴Hg was obtained from Oak Ridge National Laboratory (Oak Ridge, TN) as Hg (II) oxide, 98.11% purity. The ²⁰⁴Hg tracer provides the advantage of using isotope ratios to account for extraction inefficiencies (assuming all isotopes undergo equivalent inefficiencies). HgO was dissolved in 25 mL 69% (w/w) HNO₃ (Fisher, Pittsburgh, PA, USA) and diluted with Milli-Q water (Millipore, Bedford, MA) to a final concentration of 1.64 ppm. This primary standard was diluted as needed for spiking water and sediment sub-samples.

Sediment and water samples were subdivided within 12 hours of collection under Ar atmosphere in a bench top glove box. Seven sediment sub-samples represented 12, 24,

48, and 72 hour incubations, a non-spiked control, as well as initial methyl mercury (MeHg) and initial total mercury (THg). For sediment, an additional sub-sample was taken for analyses of total solids (TS) and percent loss on ignition (LOI), a measure of sediment organic matter. TS and LOI analyses are described in the Supporting Information. For water, one additional sub-sample was used for major ion analyses.

During sub-sampling of sediment, anoxic water overlying the sediment samples was decanted under Ar atmosphere (glove box) into a beaker. The top ~2-3 cm of the sediment was poured into a 100 mL glass beaker and stirred with a plastic spatula with addition of decanted anoxic water to yield a slurry volume of ~80 cm³. Approximately 1 g of slurry was measured into each of eight 50-mL high-speed PPCO tubes (Nalgene, Oak Ridge, TN) and ~50 g into a polypropylene centrifuge tube for TS and LOI analyses. The spatula was rinsed with Milli-Q water and dried with a Kim Wipe between each sample. For water sub-samples, approximately 100 mL of sampled water was poured under Ar atmosphere into each of eight 125-mL FLPE bottles, one 125-mL LDPE bottle, and one 125-mL amber glass bottle.

For water and sediment samples, ²⁰⁴Hg²⁺ was added to the 12, 24, 48, and 72 hour incubation samples using volumes and concentrations of diluted primary standard provided in the Supporting Information. Spiked and control sub-samples were capped and sealed with electrical tape, and placed in N₂ pressured vessels on a shaker table

rotating at ~120 rpm. Sub-samples for ambient THg and MeHg concentrations were placed in a -20°C freezer.

Following incubation, sediment and water samples were frozen (-20°C), with water having first been acidified with trace metal grade HCl to approx. 1% (v/v). Sediment and water samples were analyzed within 1.5 months and 3 months of collection, respectively. Water samples were not collected from FBS during fall since water depths were only 10 cm.

Because increased temperature drives increased SRB activity and methylation (e.g. 1), the incubation of samples at laboratory temperature is a concern. Temperature during incubation has been handled in various ways: some studies have maintained *in situ* temperatures (e.g. 6) while others have allowed samples to incubate at laboratory temperature (e.g. 5, 7). Pond temperatures spanned the laboratory temperature (~22°C), with fall water temperatures being ~15°C lower than summer water temperatures (Supporting Information). Since the goal was to understand attributes other than temperature that drive spatial variations in methylation, the same incubation temperature (laboratory) was used for all samples to minimize effects on microbial processes due to temperature differences.

Hg Extraction from Sediment and Distillation from Water

The method of extraction of organo-Hg species (including MeHg) from sediment was modified from Bloom *et al.* (17). The 1 g sediment slurries in PPCO tubes were thawed and 5 mL of 18% (w/v) KBr (ACS grade, Sigma-Aldrich, St. Louis, MO) + 5% (v/v) H₂SO₄ (trace metal grade, Fisher, Pittsburgh, PA, USA) and 1 mL 1M CuSO₄ (Sigma-Aldrich, St. Louis, MO) was added and allowed to react for 1 hour. Methylene chloride (10-20 mL) (HPLC grade, Spectrum, New Brunswick, NJ, USA) was added and vigorously shaken for 1 hour. Samples were then centrifuged for 30 minutes at 3000 rpm to separate the acid and organic solvent. A 2-mL aliquot of the organic solvent containing the extracted species was removed by pipette and diluted to 50 mL with pure water (MilliQ, Millipore Inc., Billerica, MA) in a Teflon distillation vial and evaporated to remove methylene chloride at 47°C for 30 min. The final aqueous solution was analyzed for MeHg as described below.

The method of extraction of THg from sediment was modified from Bloom *et al.* (17) and Heyes *et al.* (18). The 1-g sediment slurries in PPCO tubes were thawed and 5 mL of a 7:3 mixture of HNO₃:H₂SO₄ (both trace metal grade, Fisher, Pittsburgh, PA, USA) was added and allowed to reflux at 80°C for 6 hours. Following reflux, 40 mL of pure water was added to the acid-sediment mixture for THg analysis as described below.

Distillation of MeHg from thawed water samples prior to MeHg analyses was performed according to (19). Thawed water samples (25 mL) were diluted with milli-Q water to approximately 50 mL in a Teflon distillation vial. Ammonium pyrrolidine

dithiocarbamate (1% w/w) (Alfa Aesar, Ward Hill, MA) (200 μ L) was added to complex Hg(II) and inhibit volatilization during the distillation process and enhance recovery (19). The sample was distilled for \sim 2 hrs at 130°C. Analysis of the distillate for MeHg from water samples was performed as described below.

Hg Analyses

MeHg and THg were measured via cold vapor atomic fluorescence spectrophotometry (CVAFS) (Model III, Brooks Rand Inc., Seattle, WA) in line with inductively-coupled plasma mass spectrometry (ICP-MS) (7500ce, Agilent, Santa Clara, CA). Details of CVAFS-ICP-MS analyses are provided in the Supporting Information.

MeHg and THg analyses were performed according to EPA Methods 1630 (20) and 1631e (21), respectively. At a minimum, matrix spike recoveries and replicates were analyzed for every 10 samples. Detection limits for THg and MeHg in water, reported as three times the standard error of filter blanks (e.g. 22), are 0.1 ng/L and 4 μ g/L, respectively. Spike recovery for MeHg in water was $84\pm 15\%$ (n=29). Spike recovery for THg in water was $109\pm 4\%$ (n=4). RSD of replicates was 17% for MeHg (n = 29) in water and 3.5% for THg in water (n = 4).

Certified reference material (CRM), used as a proxy for MeHg recovery from sediment, was CC580 estuarine sediment standard (European Reference Materials Institute for Reference Materials and Measurements, Geel, Belgium). Measured recovery of MeHg

from CC580 was $70.6 \pm 16.6\%$ ($n=10$). For THg, the CRM used was MESS-3 (Canadian National Research Council, Ottawa, Ontario, Canada) marine sediment from the Beaufort Sea. Recovery for THg from MESS-3 was $106 \pm 11\%$ ($n=7$).

Kinetic Model for Methylation Rates

Methylation rate coefficients were backed out from observed changes in isotope ratios during incubation. Defining:

$$R_{MeHg}^{202/204} = \frac{[^{202}MeHg]}{[^{204}MeHg]}$$

where the brackets refer to observed masses (counts) of specific MeHg isotopes during CVAFS-ICP-MS.

Assuming that no gaseous Hg is present, then inorganic Hg was equal to the difference between THg and MeHg, and the rate of change of inorganic Hg concentration is opposite to the rate of change of MeHg concentration:

$$\frac{d[Me^{204}Hg]}{dt} = k_{meth}[T^{204}Hg - Me^{204}Hg] - k_{demeth}[Me^{204}Hg]$$

where the brackets refer to concentrations, and where k_{meth} and k_{demeth} are conditional first order rate coefficients for methylation and demethylation, respectively. The term conditional reflects the fact that these kinetic rate constants are dependent on multiple factors (e.g., dissolved organic carbon in pore water, sediment organic matter, sulfate bioavailability, SRB activity, etc.) that were not explicitly considered in the simple first order kinetic model above.

In terms of isotope ratios:

$$\frac{d}{dt} R_{MeHg}^{202/204} = \frac{d}{dt} \left[\frac{Me^{202}Hg}{Me^{204}Hg} \right] = \frac{k_{meth} [T^{202}Hg - Me^{202}Hg]}{k_{meth} [T^{204}Hg - Me^{204}Hg]} - \frac{k_{demeth} [Me^{202}Hg]}{k_{demeth} [Me^{204}Hg]}$$

Performing numerical approximation yields the change in the ratios as a function of time:

$$R_{MeHg}^{202/204}(t) = \frac{[MeHg]_{t-1}^{202} + k_{meth} [THg - MeHg]_{t-1}^{202} \Delta t - k_{demeth} [MeHg]_{t-1}^{202} \Delta t}{[MeHg]_{t-1}^{204} + k_{meth} [THg - MeHg]_{t-1}^{204} \Delta t - k_{demeth} [MeHg]_{t-1}^{204} \Delta t}$$

where Δt is the time step between observations.

Values of k_{meth} and k_{demeth} were backed out by implementing the above equation on a spreadsheet and comparing to the time series of values of $R_{MeHg}^{202/204}$. Initial values for $Me^{202}Hg$, $Me^{204}Hg$, $T^{202}Hg$, and $T^{204}Hg$ were determined by cross calibration of CVAFS and ICP-MS, and are provided in the Supporting Information. Additional constraint for model fits was provided by the requirement for the model to match observed general trends and magnitudes of measured $M^{202}Hg$ and $M^{204}Hg$ counts. Example figures showing best, lower, and upper model fits to measured data (accounting for 70% recovery from sediment CRMs) are also provided in the Supporting Information.

Results

Methylation rates

The ratio of $^{202}\text{Hg}/^{204}\text{Hg}$ for both THg and MeHg in unspiked samples was close to 4.35 (reflecting natural abundances); whereas, addition of the $^{204}\text{Hg}^{2+}$ spike (incubation time > 0) decreased $R^{202/204}_{\text{THg}}$ below ambient values. Methylation in sediment samples was reflected in the observed subsequent decrease in $R^{202/204}_{\text{MeHg}}$ during incubation (Figure 2), whereas unspiked controls, incubated 72 hours, (Figure 2 and Table 1) maintained natural values of $R^{202/204}_{\text{MeHg}}$ (Figure 2 and Table 1). Notably, in two samples (FBS-5 and FBN-4) the unspiked controls yielded values significantly lower than natural; however, for both samples, only insignificant decreases in $R^{202/204}_{\text{MeHg}}$ were observed. The contrasting values of $R^{202/204}_{\text{MeHg}}$ between sediment samples and unspiked controls indicate that the analytical methods did not produce artifact-driven decreases in $R^{202/204}_{\text{MeHg}}$ in samples where significant decreases were observed.

Table 1. $R^{202/204}_{\text{MeHg}}$ in unspiked controls and 72-hour samples.

Transect		FBN Summer				
Site	FBN-1	FBN-2	FBN-3	FBN-4	FBN-5	
control	4.231	4.375	4.487	4.381	4.085	
72 hour	0.931	2.359	3.483	1.159	4.169	

Transect		FBN Fall			
Site	FBN-1	FBN-2	FBN-3	FBN-4	
control	4.164	4.232	4.282	3.657	
72 hour	0.778	1.398	1.926	3.563	

Transect		OB Summer				
Site	OB-1	OB-2	OB-3	OB-4	OB-5	
control	4.298	4.583	4.358	4.406	4.332	
72 hour	3.669	1.803	2.865	3.202	1.214	

Transect		FBS Summer				
Site	FBS-1	FBS-2	FBS-3	FBS-4	FBS-5	
control	4.376	4.264	4.393	4.187	3.598	
72 hour	4.395	4.353	4.361	4.409	4.321	

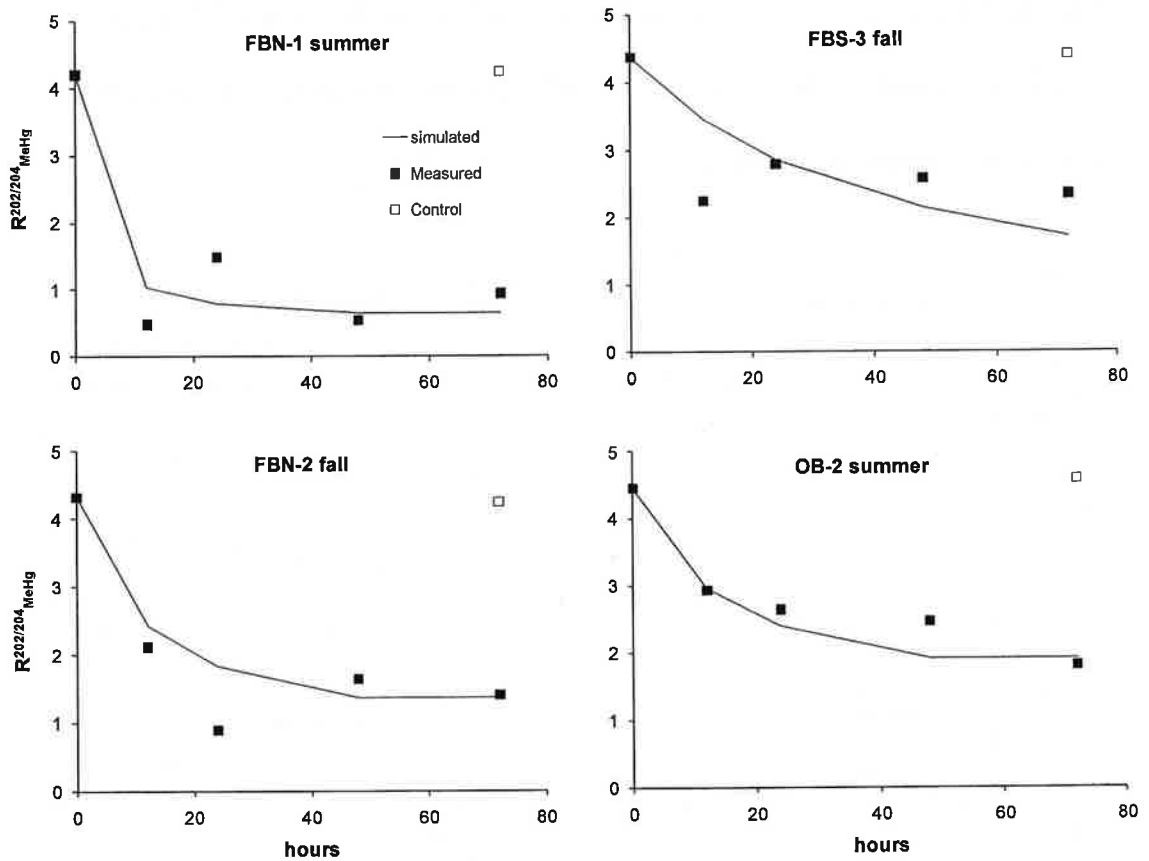


Figure 2. Values of $R^{202/204}_{MeHg}$ across the time series for all four transects. Value of $R^{202/204}_{MeHg}$ for the unspiked control for each transect sample set. Value of $R^{202/204}_{THg}$ in spiked subsample for each transect sample set. Lines show best fits of kinetic simulations using criteria described in Methods section.

Concentrations of $Me^{202}Hg$ and $Me^{204}Hg$ increased measurably after 24 hours of incubation (Figure 3), and then decreased from 48 to 72 hours, possibly indicating that demethylation became the dominant process following depletion of a critical reagent such as sulfate or labile organic matter or labile Hg. This general trend in MeHg concentrations allowed further constraint on backing out k_{meth} , by inclusion of k_{demeth} to fit these general trends (Figure 3) accounting for 70% recovery from CRMs.

Notably, the kinetic expression was unable to simulate the observed $R^{202/204}_{MeHg}(t)$ under the assumption that only spiked $^{204}Hg^{2+}$ was labile, indicating that both ambient and spiked Hg were methylated.

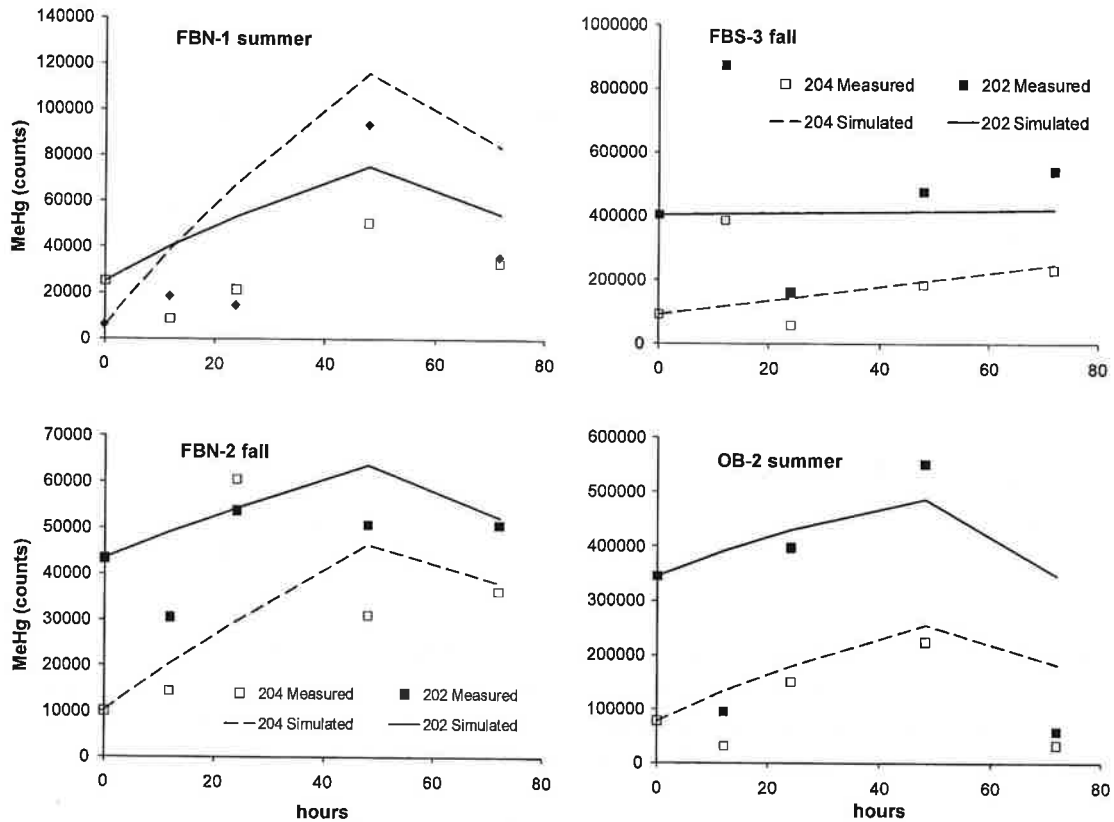


Figure 3. Measured counts $^{204}MeHg$ and $^{202}MeHg$ across the time series for all four transects. Lines show best fits of kinetic simulations using criteria described in Methods section.

No significant change in $R^{202/204}_{MeHg}$ was observed for water column samples, indicating that methylation occurred predominantly in the underlying sediment. FBS summer sediment samples also showed no methylation; however, this may reflect a low spike

mass addition relative to ambient THg in the sample (1.8 - 5.0%), as described in the Supporting Information.

Sediment methylation rates (k_{meth}) were generally higher in transects FBN and OB relative to FBS (Figure 4, and Supporting Information) with values ranging over three orders of magnitude from approximately $1E-6$ to $1E-3$. Demethylation rate coefficients (k_{demeth}) were generally two to three orders of magnitude higher than methylation rate coefficients, and in transect FBN they were proportional to methylation rate coefficients.

Spatial trends in k_{meth} corresponded well with spatial trends in sediment organic matter content (%LOI) (Figure 4) for transects FBN and OB. In terms of field water column parameters (described below) spatial trends in k_{meth} and k_{demeth} did not match spatial trends observed for water column salinity (conductance or sulfate) or DO (Figures 4 and 5). However, the lowest methylation potential for FBN summer did correspond to the location of a brine wedge (Figures 4 and 5), possibly indicating an inhibiting effect of the ephemeral brine wedge on methylation during that period.

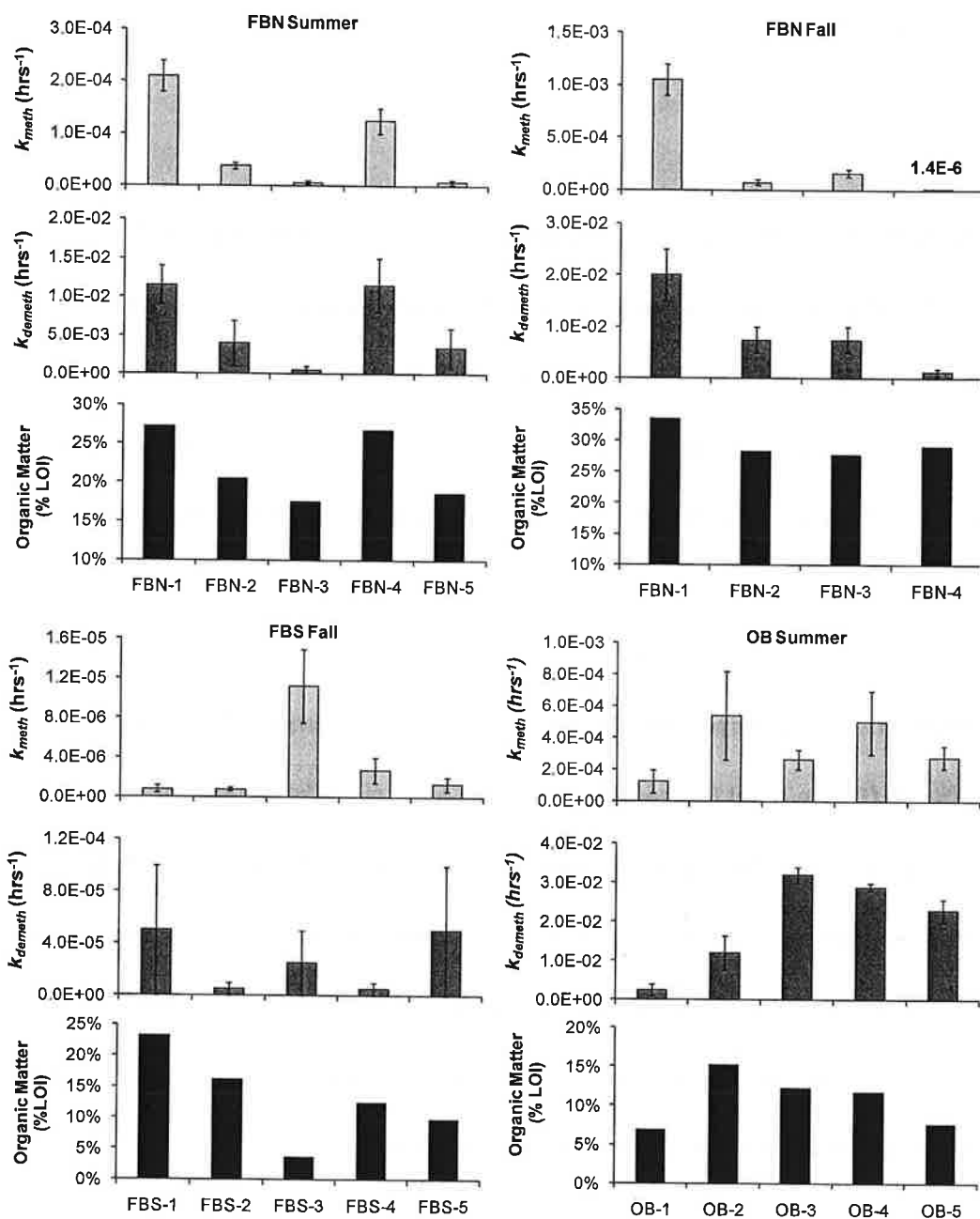


Figure 4. Spatial trends in kinetic rate coefficients (k_{meth} , k_{demeth}) compared to spatial trends in sediment organic matter content (%LOI).

Field Parameters

Within each transect the water chemistry was relatively constant, whereas a range from fresh to saline conditions existed between the transects (Figure 5, and Supporting

Information). FBS was relatively fresh, whereas OB was saline, and FBN was intermediate, with typical conductivities of a few thousand, few hundred thousand, and tens of thousands $\mu\text{S}/\text{cm}$, respectively (Figure 5). The variation in pH between the transects was relatively small, with typical ranges of 7.3 to 8.3 (FBS), 7.4 to 7.9 (OB), and 9.2 to 9.6 (FBN) (Supporting Information). Notable deviations of pH down to 8.1 for FBN (deeper samples) during summer 2009 corresponded to saline water intrusion through the causeway opening as described below. Water temperatures were generally higher, and DO concentrations were generally lower, during summer relative to fall, reflecting the influence of increased microbial respiration with increased temperature (Supporting Information). DO concentrations also tended to be lower at sampling points closer to the sediment surface (Figure 5), and sulfide was present (0.7 to 2.5 mg/L) in the near-sediment water during summer conditions at FBN (Supporting Information). The center of FBN corresponds to a location where bi-directional flow occurs through an opening in the auto causeway that parallels the transect (Figure 1). Corresponding to these center sites, the deeper water (>0.7 fractional depth) conductivities and sulfate concentrations were relatively elevated, $> 10^5 \mu\text{S}/\text{cm}$, and $> 6700 \text{ mg}/\text{L}$, respectively (Figure 5), reflecting a saline wedge of water pushed into Farmington Bay from the main body of GSL through the auto-causeway bridge by a northerly wind on the day of sampling. Notably, DO and sulfide coexist in the water column at FBN, likely representing the combined influences of the water-air interface, the brine-fresh water interface, and the sediment-water interface in this relatively shallow water column.

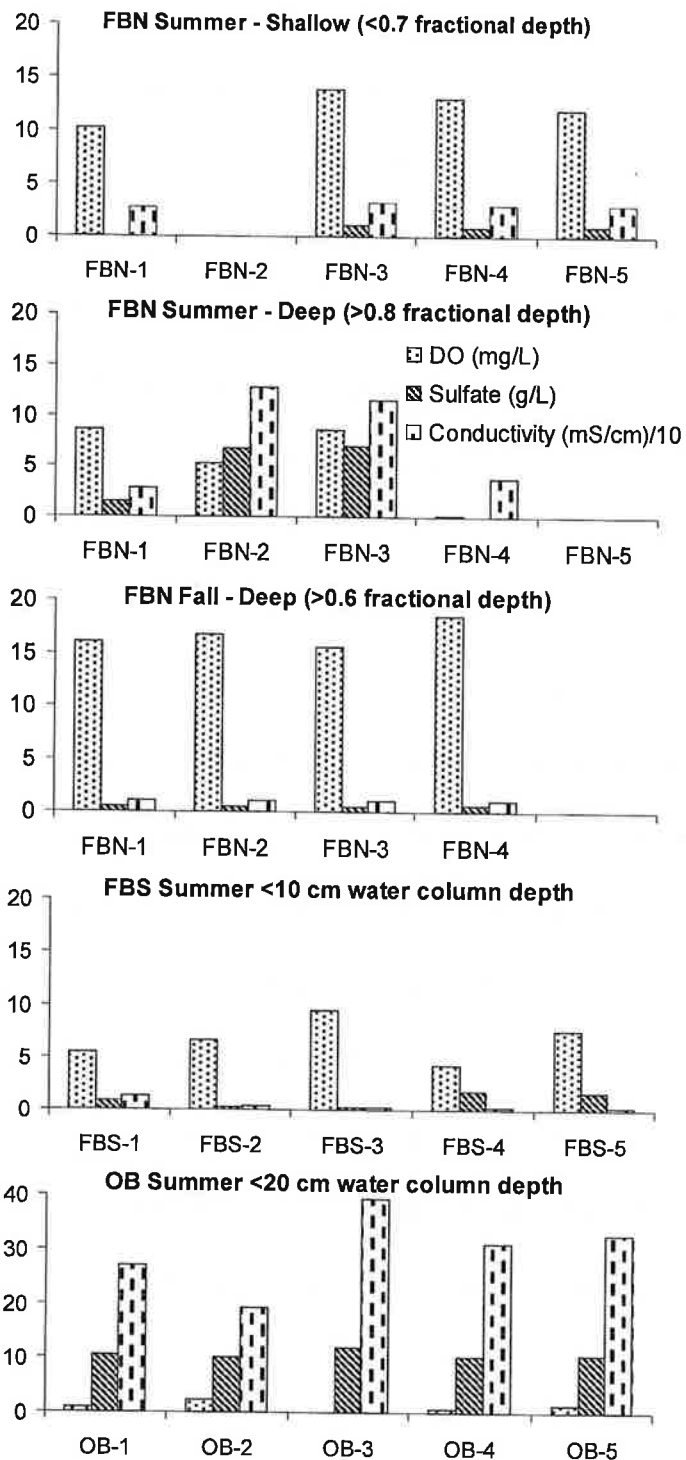


Figure 5. Spatial trends in field parameters for all transects (see Supporting Information for tabular values). Parameters shown include DO (mg/L), sulfate (g/L), and conductivity (units converted to millisiemens per cm divided by 10 for scaled comparison). Sulfate was analyzed in the laboratory following sub-sampling. Y-axis units are different for all parameters and are shown in the legend.

Total and methyl mercury

Measured MeHg and THg concentrations are shown in Figure 6, whereas tabular values are given in the Supporting Information. Significant variations in MeHg and THg concentrations were observed within and between the transects; however, it should be noted that the water column samples were unfiltered, and so are subject to the variability that may arise from inclusion of particulate phases. Water column MeHg ranged from less than 1% up to 39% of THg; whereas, this ratio was less than 2% in sediment, for all transects (Figure 6, and Supporting Information). Some water column THg, and all MeHg concentrations, were significantly decreased in fall relative to summer at FBN (Figure 6), where seasonal variations were examined. FBN summer water column THg concentrations decreased from west to east, with MeHg roughly following this trend. In contrast, FBN summer sediment THg and MeHg concentrations increased from west to east (Figure 6). FBN-5 was not sampled in fall due to water depth <30 cm (access difficulty).

Spatial trends in FBN THg and MeHg concentrations, in both water column and sediment, were not similar to spatial trends observed for salinity (conductivity, sulfate) or DO (compare Figures 5 & 6), sediment organic matter content (compare Figures 5 & 6), or DOC (Supporting Information). The shallow sample from FBN-3 showed virtually the same MeHg and THg concentrations during summer and fall, indicating that THg and MeHg concentrations did not correspond to the presence versus absence of the brine wedge. No clear spatial trends were observed for THg and MeHg in the OB and FBS transects, except that the highest THg

concentrations in sediment and water occurred at site FBS-2, adjacent to the Jordan River outflow (Figures 1 & 6).

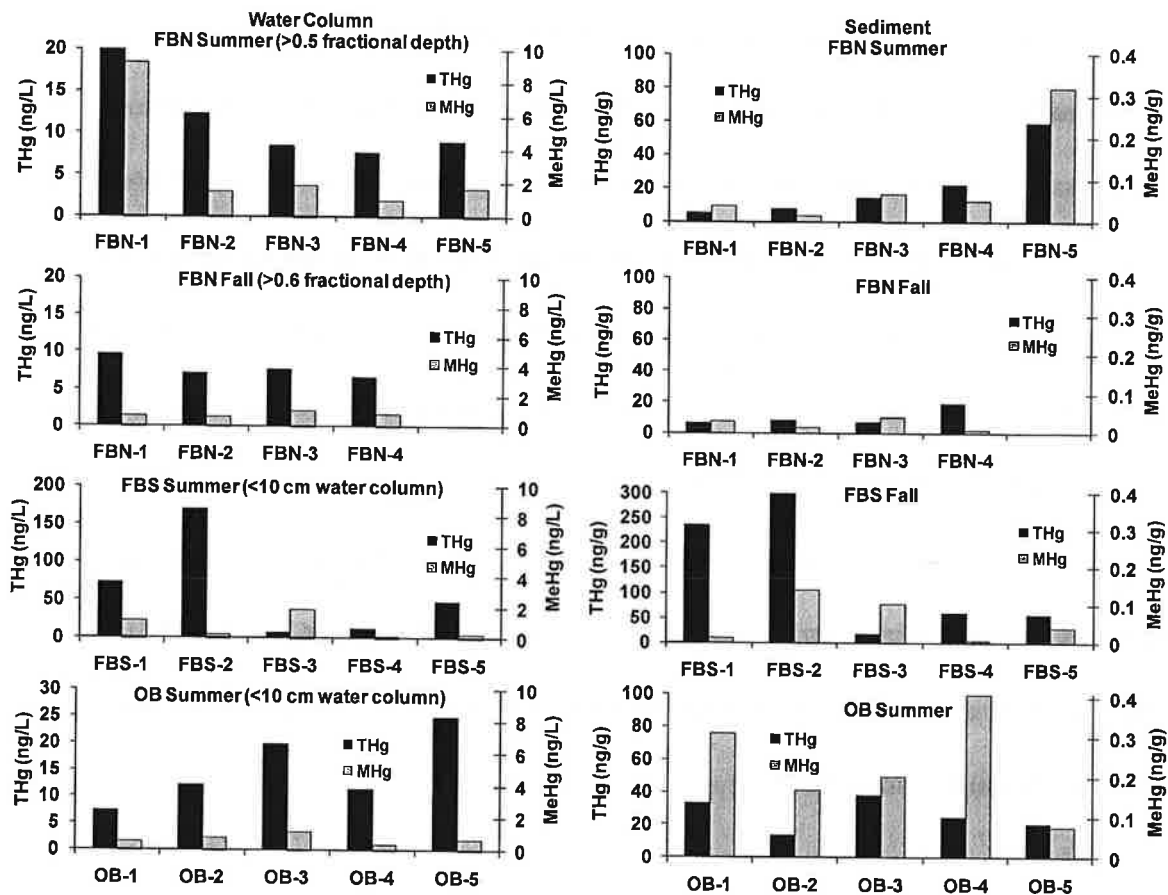


Figure 6. Spatial trends in initial, un-spiked THg and MeHg concentrations in water column and sediment samples.

Discussion

Correlations

The observed spatial variability of MeHg in sediment (Figure 6) and methylation rate constants in sediment (Figure 4) warrant investigation to determine what parameters may relate to this spatial distribution. Considering first the production of methyl mercury, i.e. methylation rates (k_{meth}), we observed significant spatial correspondence to sediment organic matter content

(%LOI) (Figure 4) for transects OB summer, FBN summer, and FBN fall, which generally showed higher methylation rate constants relative to FBS. The methylation rate constants (k_{meth}) for two of the transects: FBN summer and OB summer were significantly correlated to sediment organic matter content (Figure 7), with $R^2 = 0.895$ and 0.672 , respectively, and $P = 0.015$ and 0.089 , respectively. Ninety-percent confidence intervals are provided for FBN summer and OBN summer in Figure 7. Notably, the relatively high R^2 for FBN fall results from a single outlier, and the correlation is not significant at the 10% confidence level. However, the FBN summer and OB summer correlations suggest a role of sediment organic matter in regulating the production of MeHg in these GSL bays.

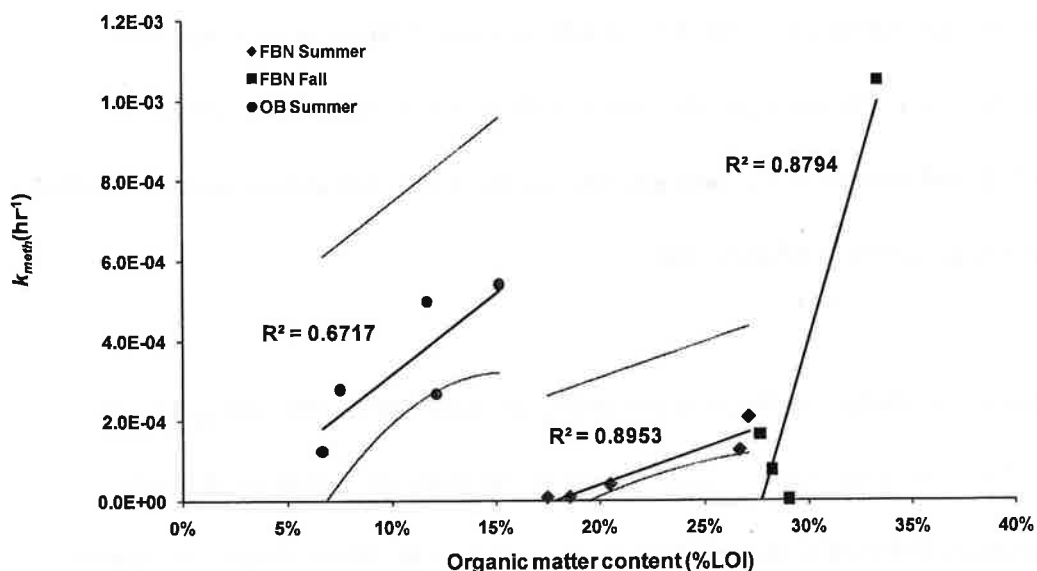


Figure 7. Linear regressions correlating methylation rate (k_{meth}) to sediment organic matter content for transects FBN summer, FBN fall, and OB summer. Confidence intervals (90%) shown for FBN summer and OB summer.

Positive correlation between %LOI and k_{meth} was previously reported (4, 5), leading to the possibility that sediment organic content may be a good predictor of spatial trends in

methylation rates. However, when the methylation rate constants from the various transects examined here are grouped together, the correlation disappears, indicating that other factors in addition to sediment organic matter content (e.g. organic matter lability, sulfide concentrations, among others) influence the methylation rate constant. Whereas sediment organic matter content appears to influence methylation for a specific transect (area), other controlling factors must be identified in order to predict methylation rate constants across the larger system.

Spatial correspondence of MeHg and THg in water and sediment has been observed in previous studies (e.g. 1, 2, 3). Such correspondence was observed in transect FBN during summer 2009 (Figure 6) with direct THg:MeHg correlations having R^2 values of 0.94 (sediment) and 0.92 (water column). However, this correspondence was only weakly indicated at transect OB summer ($R^2 = 0.12$), and the correlation was actually inverse at FBN fall, and no such correlation was observed in FBS (Supporting Information).

Regular spatial trends in MeHg and THg concentrations are apparent at FBN, with generally higher values in the water column at the western end of the transect, and generally higher values in the sediment at the eastern end of the transect (Figure 6). Weak direct correlations between sediment organic matter content and sediment THg, as well as between water column DOC and water column THg (Supporting Information), suggest an influence of organic matter on THg spatial distribution in FBN. Previous studies have suggested a direct relationship between sediment MeHg and sediment organic carbon concentrations (2, 3, 4).

The observed lack of correlation between k_{meth} and MeHg concentration in our study (compare Figures 4 and 6) is consistent with results in Drott *et al.* (7) for sediments underlying brackish surface water. In contrast to the expectations of Rolffhus *et al.* (9), there was no clear correlation between water column salinity and any of the methylation-related parameters such as k_{meth} or MeHg concentration or THg concentration within a given transect for either the sediment or water column (Supporting Information). However, correlation between k_{meth} and salinity is qualitatively observed when the data was grouped by location, where the higher salinity locations, i.e. OB and FBN showed greater methylation rate constants relative to the lower salinity transect FBS.

Values for methylation rate constant in our study ranged from $1.1E-3$ to $8.0E-7$ (hrs^{-1}), indicating that the lower k_{meth} values observed in Farmington Bay were a factor of 10 below those in reported Drott *et al.* (7) for contaminated sediments from eight highly geochemically variable sites (e.g. small fresh water lakes to large brackish estuaries) ranging from $8.3E-4$ to $8.3E-6$ hrs^{-1} . Converting our constants to units of $ng \cdot g^{-1} \cdot day^{-1}$ yields methylation rate constants that range from $2.6E-2$ to $1.0E-6$ $ng \cdot g^{-1} \cdot day^{-1}$ (Supporting Information), which are lower (2 to 5 orders of magnitude) than those reported by Lambertsson and Nilsson (4), which ranged from 2.3 to 0.2 $ng \cdot g^{-1} \cdot day^{-1}$ in an estuarine environment.

Among the parameters examined, the clearest relationship was between sediment organic carbon content and methylation rate coefficient. Future studies will examine the spatial

variation of these parameters in the main body of the Great Salt Lake and their vertical variation among the anoxic (and organic rich) deep brine layer and underlying sediment.

Acknowledgements

This research was supported by funding from the Division of Forestry Fire, and State Lands (FFSL) of the Utah Department of Natural Resources, as well as a grant from the Tides Foundation. We would like to thank the late Dave Grierson (of FFSL) for his support, and for making this study possible. We would like to thank Leland Myers and staff at the Central Davis Sewer District for providing access to the south end of Farmington Bay and Dr. David Naftz for supplying field sampling equipment and logistical support for transect FBN.

Literature Cited

1. Benoit, J. M.; Gilmour, C. C.; Heyes, A.; Mason, R. P.; Miller, C. L., Geochemical and biological controls over methylmercury production and degradation in aquatic ecosystems. In *Biogeochemistry of Environmentally Important Trace Elements*, Cai, Y.; Braids, O. C., Eds. Amer Chemical Soc: Washington, 2003, 835, 262-297.
2. Sunderland, E. M.; Gobas, F.; Branfireun, B. A.; Heyes, A., Environmental controls on the speciation and distribution of mercury in coastal sediments. *Marine Chemistry* 2006, 102, (1-2), 111-123.
3. Hammerschmidt, C. R.; Fitzgerald, W. F., Geochemical controls on the production and distribution of methylmercury in near-shore marine sediments. *Environmental Science & Technology* 2004, 38, (5), 1487-1495
4. Lambertsson, L.; Nilsson, M., Organic material: The primary control on mercury methylation and ambient methyl mercury concentrations in estuarine sediments. *Environmental Science & Technology* 2006, 40, (6), 1822-1829.
5. Marvin-DiPasquale, M. M. D.; Lutz, M. A.; Brigham, M. E.; Krabbenhoft, D. P.; Aiken, G. R.; Orem, W. H.; Hall, B. D., Mercury Cycling in Stream Ecosystems. 2. Benthic Methylmercury Production and Bed Sediment-Pore Water Partitioning. *Environmental Science & Technology* 2009, 43, (8), 2726-2732.
6. Hammerschmidt, C. R.; Fitzgerald, W. F., Methylmercury cycling in sediments on the continental shelf of southern New England. *Geochimica et Cosmochimica Acta* 2006, 70, (4), 918-930.
7. Drott, A.; Lambertsson, L.; Bjorn, E.; Skyllberg, U., Do potential methylation rates reflect accumulated methyl mercury in contaminated sediments? *Environmental Science and Technology* 2008, 42, (1), 153-158.
8. Hollweg, T. A.; Gilmour, C. C.; Mason, R. P., Methylmercury production in sediments of Chesapeake Bay and the mid-Atlantic continental margin. *Mar. Chem.* 2009, 114, (3-4), 86-101.
9. Rolfhus, K. R.; Lamborg, C. H.; Fitzgerald, W. F.; Balcom, P. H., Evidence for enhanced mercury reactivity in response to estuarine mixing. *Journal of Geophysical Research* 2003, 108, (C11), 17-1.
10. Great Salt Lake; <http://www.whsrn.org/site-profile/great-salt-lake>
11. Aldrich, T. W.; D. S. Paul., Avian ecology of Great Salt Lake in Gwynn, J.W., ed. *Great Salt Lake: an overview of change*. Utah Department of Natural Resources Special Publication 2002, 343-374.
12. Scholl, D.J.; Ball, R.W., An evaluation of mercury concentrations in ducks from the Great Salt Lake, Utah for 2005 and 2006; Health Advisory Report. Utah Dept. of Health, Office of Epidemiology, Salt Lake City, UT, USA, 2006
13. Conover, M. R.; Vest, J. L., Selenium and mercury concentrations in California gulls breeding on the great Salt Lake, Utah, USA. *Environmental Toxicology and Chemistry* 2009a, 28, (2), 324-329
14. Conover, M. R.; Vest, J. L., Concentrations of selenium and mercury in eared grebes (*Podiceps nigricollis*) from Utah's Great Salt Lake, USA. *Environmental Toxicology and Chemistry* 2009b, 28, (6), 1319-1323.

15. Naftz, D.; Angeroth, C.; Kenney, T.; Waddell, B.; Darnall, N.; Silva, S.; Perschon, C.; Whitehead, J., Anthropogenic influences on the input and biogeochemical cycling of nutrients and mercury in Great Salt Lake, Utah, USA. *Applied Geochemistry* 2008, 23, (6), 1731-1744.
16. Diaz, X.; Johnson, W. P.; Fernandez, D.; Naftz, D. L., Size and elemental distributions of nano- to micro-particulates in the geochemically-stratified Great Salt Lake. *Applied Geochemistry* 2009, 24, (9), 1653-1665.
17. Bloom, N. S.; Colman, J. A.; Barber, L., Artifact formation of methyl mercury during aqueous distillation and alternative techniques for the extraction of methyl mercury from environmental samples. *Fresenius J. Anal. Chem.* 1997, 358, (3), 371-377.
18. Heyes, A.; Mason, R. P.; Kim, E. H.; Sunderland, E., Mercury methylation in estuaries: Insights from using measuring rates using stable mercury isotopes. *Marine Chemistry* 2006, 102, (1-2), 134-147.
19. Bloom N, Horvat M, Watras CJ. Results of the international aqueous mercury speciation intercomparison exercise. (Originally published in *Water, Air, and Soil Pollution* 80: 1257-1268, 1995): Kluwer Academic Publishers; Kluwer Academic Publishers, 1995.
20. US EPA Method 1630: Methylmercury in water by distillation, aqueous ethylation, purge and trap, and CVAFS; U.S. EPA: WA, DC, 2001b.
21. US EPA Method 1631, Revision E: Mercury in water by oxidation, purge and trap, and cold vapor atomic fluorescence spectrometry; U.S. EPA: WA, DC, 2002.

1
2
3
4
5
6
7
8
9
10

Supporting Information for:

**Spatial variation of mercury methylation in Farmington and Ogden Bays, Great
Salt Lake, UT: correlation to organic matter content in sediment**

Abigail Rudd, Diego P. Fernandez,

Gregory T. Carling, and William P. Johnson *

Dept. of Geology & Geophysics

University of Utah, Salt Lake City, UT 84112

* Corresponding author. Email: william.johnson@utah.edu. Tel: (801)585-5033. Fax: (801)581-7065.

1 *Field parameters, sulfide, major ions*

2 Water quality parameters (T, pH, DO, and conductivity) as well as sulfide and major anions (F⁻,
3 Cl⁻, NO₃⁻, SO₄²⁻) were measured using multi-parameter probes; Troll 9500 (In Situ Inc., Ft.
4 Collins, CO, USA), or YSI Pro Plus (YSI Inc., Yellow Spring, OH), which were calibrated
5 immediately prior to sampling. Water samples were collected via a peristaltic pump with acid-
6 washed PTFE tubing in 1L FLPE bottles filled to overflowing, tightly capped and taped (electrical)
7 to prevent exposure to air. Parallel samples were filtered (0.45 µm, polyethersulfone) in-line
8 and immediately tested for sulfide (methylene blue method) using a CHEMetrics V-2000 Multi-
9 analyte LED Photometer and Vacu-vials[®]. Major anions (F⁻, Cl⁻, NO₃⁻, SO₄²⁻) were analyzed
10 following laboratory sub-sampling using a Dionex 4100 ion chromatograph. Dissolved organic
11 carbon analyses were performed from water samples from two of the transects (FBN summer
12 and FBS summer), as described below.

13
14 *DOC Analyses*

15 Prior to analysis, water samples from FBN summer and OB summer were filtered using a glass
16 filtration apparatus and pre-fired glass fiber 0.45 µm filters (Advantec Grade GF75) or
17 Whatman 0.45 µm PES syringe filters. DOC samples were analyzed within three weeks of
18 collection using a Shimadzu TOC- 5000A. Fresh standards were created prior to analysis with
19 potassium hydrogen phthalate for total carbon and sodium hydrogen carbonate and sodium
20 carbonate for inorganic carbon. Organic carbon in samples was calculated as the difference
21 between total and inorganic carbon.
22

23 *Total Solids and Total Volatile Solids Analysis*

24 Sediment slurries were analyzed for total solids (TS) and total volatile solids (TVS)
25 according to EPA Method 1684 (US EPA Method 1684: Total, Fixed, and Volatile Solids in Water,
26 Solids, and Biosolids; U.S. EPA: WA, DC, 2001a.). Approximately 25 g of sediment slurry was
27 poured into porcelain evaporating dishes, which had been ignited to 550°C in a muffle furnace
28 to a constant empty weight prior to analysis. Samples were dried overnight (for approximately
29 12 hours) at 104°C, placed in a desiccator and cooled before weighing. The samples were then
30 combusted at 550°C in a muffle furnace for approximately two hours, allowed to cool in a
31 desiccator, then weighed. The following equations were used to calculate TS and TVS:

32
$$TS = \frac{W_{total} - W_{dish}}{W_{sample} - W_{dish}} * 100 \quad (1)$$

33
$$TVS = \frac{W_{total} - W_{volatile}}{W_{total} - W_{dish}} * 100 \quad (2)$$

34 where W_{dish} is the weight of dish (mg), W_{sample} is the weight of wet sample and dish (mg), W_{total}
35 is the weight of dried residue and dish (mg), and $W_{volatile}$ is the weight of residue and dish after
36 ignition (mg).

Transect	Farmington Bay North Summer									
Site	FBN-1			FBN-2	FBN-3		FBN-4		FBN-5	
Water Depth (m)	1			1	1		0.75		0.4	
Sample Depth (m)	0.4	0.8	1	0.9	0.2	0.9	0.5	0.75	0.2	
Water Temp (°C)	25.28	25.14	24.37	25.16	27.34	26.29	26.67	26.2	27.21	
pH	9.49	9.41	9.08	8.14	9.6	8.28	9.54	8.48	9.31	
Conductivity (µS/cm)	27440	27790	29150	127500	31910	115200	29880	37810	29080	
DO (mg/L)	10.16	8.6	0.96	5.22	13.89	8.56	12.98	0.11	11.9	
S ²⁻ (mg/L)	nm	2.5	nm	0.7	<DL	0.7	<DL	nm	nm	
SO ₄ ²⁻ (mg/L)	1429			6752	1010	7000	885		967	
DOC (mg/L)	56.75			64.29	39.29	57.54	34.00		39.63	
Transect	Farmington Bay North Fall									
Site	FBN-1			FBN-2	FBN-3		FBN-4			
Water Depth (m)	0.7			0.9	1		0.3			
Sample Depth (m)	0.511			0.59	0.57		0.272			
Water Temp (°C)	8.59			9.01	9.13		10.03			
pH	9.2			9.53	9.6		9.51			
Conductivity (µS/cm)	10690			10670	10720		10800			
DO (mg/L)	16.01			16.73	15.57		18.46			
S ²⁻ (mg/L)	<DL			<DL	<DL		<DL			
SO ₄ ²⁻ (mg/L)	505.2			524.1	529.0		533.5			
DOC (mg/L)	nm			nm	nm		nm			
Transect	Farmington Bay South Summer									
Site	FBS-1			FBS-2	FBS-3		FBS-4		FBS-5	
Water Depth (m)	<10 cm			<10 cm	<10 cm		10 cm		<10 cm	
Sample Depth (m)	0.065			0.07	0.083		0.085		0.064	
Water Temp (°C)	17.73			22.46	23.01		22.85		27.73	
pH	8.03			7.26	8.28		7.52		8.14	
Conductivity (µS/cm)	13270			2988	2650		1892		2323	
DO (mg/L)	5.41			6.58	9.47		4.24		7.59	
S ²⁻ (mg/L)	<DL			<DL	<DL		<DL		<DL	
SO ₄ ²⁻ (mg/L)	856.7			252.3	220.2		177.9		160.3	
DOC (mg/L)	nm			nm	nm		nm		nm	
Transect	Ogden Bay									
Site	OB-1			OB-2	OB-3		OB-4		OB-5	
Water Depth (m)	0.08			0.08	0.05		0.15		0.18	
Sample Depth (m)	0.06			0.06	0.03		0.1		0.1	
Water Temp (°C)	17.5			20.2	28.6		24.2		26.2	
pH	7.85			7.86	7.45		7.78		7.86	
Conductivity (µS/cm)	269411			192958	392021		311975		325932	
DO (mg/L)	0.99			2.4	0.03		0.68		1.26	
S ²⁻ (mg/L)	<DL			<DL	<DL		<DL		<DL	
SO ₄ ²⁻ (mg/L)	nm			nm	nm		nm		nm	
DOC (mg/L)	32.9			37.7	57.1		55.0		60.3	

(nm = not measured, DL = detection limit). S²⁻ DL = 0.2 mg/L; SO₄²⁻ DL = 0.5 mg/L.

Table S1. Added ^{204}Hg spike concentration (ppb), volume (mL), and mass (ng) for all samples shown with the measured (pre-spike) total Hg (THg) mass (ng) and the ratio of added Hg from the spike to ambient Hg.

Transect	Sample Type	Sample	^{204}Hg Spike			Sample Total Hg (pre-spike) (ng)	Spike/ Ambient THg %
			Conc. (ppb)	Volume (mL)	Mass (ng)		
North Summer	sediment	FBN-1	36.5	0.100	3.65	6.36	57.4
		FBN-2	36.5	0.100	3.65	7.00	52.1
		FBN-3	36.5	0.100	3.65	15.6	23.3
		FBN-4	36.5	0.100	3.65	21.8	16.8
		FBN-5	36.5	0.100	3.65	58.8	6.2
	water	FBN-1	0.30	0.500	0.15	2.34	6.4
		FBN-2	0.30	0.500	0.15	1.23	12.2
		FBN-3 0.2m	0.30	0.500	0.15	0.84	17.8
		FBN-3 0.9m	0.30	0.500	0.15	0.85	17.6
		FBN-4	0.30	0.500	0.15	0.77	19.6
South Summer	sediment	FBS-1	36.5	0.100	3.65	127	2.9
		FBS-2	36.5	0.100	3.65	204	1.8
		FBS-3	36.5	0.100	3.65	85.0	4.3
		FBS-4	36.5	0.100	3.65	73.6	5.0
		FBS-5	36.5	0.100	3.65	88.0	4.1
	water	FBS-1	0.30	0.500	0.15	7.22	2.1
		FBS-2	0.30	0.500	0.15	17.0	0.9
		FBS-3	0.30	0.500	0.15	0.63	24.0
		FBS-4	0.30	0.500	0.15	1.19	12.6
		FBS-5	0.30	0.500	0.15	4.73	3.2
South Fall	sediment	FBS-1	235	0.200	47.0	234	20.1
		FBS-2	235	0.200	47.0	327	14.4
		FBS-3	235	0.200	47.0	19.4	242.5
		FBS-4	235	0.200	47.0	59.4	79.1
		FBS-5	235	0.200	47.0	60.6	77.6
North Fall	sediment	FBN-1	36.5	0.050	1.83	6.44	28.3
		FBN-2	36.5	0.070	2.56	9.20	27.8
		FBN-3	36.5	0.120	4.38	6.76	64.8
		FBN-4	36.5	0.200	7.30	21.0	34.7
	water	FBN-1	1.46	0.500	0.73	0.97	75.1
		FBN-2	1.46	0.300	0.44	0.71	61.8
		FBN-3	1.46	0.200	0.29	0.77	38.2
		FBN-4	1.46	0.160	0.23	0.66	35.4

ICP-MS Chromatogram Integration and Correction and Unit Conversion

Table S2. ICP-MS and CVAFS operating conditions

ICP-MS		CV-AFS	
Plasma Conditions		Carrier Gas Conditions	
Ar Tank Pressure (psi)	701	Ar Tank Pressure (psi)	25
Ar Flow Rate (L/min)		Ar Flow Rate (mL/min)	50
carrier	1.1		
Auxillary	0.9	Instrument Conditions	
Plasma	15	Fluorescence Detector UV wavelength (nm)	254
		Trap Desorption Module (V)	10.5
		Temperature (°C)	~500
Instrument Conditions			
Vacuum (Pa)		MeHg Analyses	
I/F	273	PMT	714.2
Analyzer	1.44×10^{-4}	Offset	45996
Power (W)		Signal Noise	136
Forward	1550	GC Temperature (°C)	105
Reflected	2	Pyrolytic Column Temperature (°C)	750
Temperature (°C)			
Water	27	THg Analyses	
housing inlet	22	PMT	552.6
housing outlet	44	Offset	6002
		Signal Noise	110

Peaks from ICP-MS analyses were integrated using Agilent Offline Data Analysis software after visual identification of peak start and end points. Background area was subtracted from peak area of the MeHg signal. An output file was generated by the software with integration values for each isotope (196, 198, 199, 200, 201, 202, and 204) in counts (counts). Background correction was also done manually with the Offline Data Analysis software. Background time intervals with the same range as the MeHg peak were integrated near the MeHg peak and near the end of data collection. These values were then subtracted from the peak integration and averaged to give a final value for the MeHg peak in counts. Table S3 and S4 shows initial, unspiked counts of $M^{202}\text{Hg}$ and $M^{204}\text{Hg}$ measured by ICP-MS for all samples modeled to obtain kinetic rate coefficients.

Coupling between CVAFS and ICP-MS was performed using a PTFE end cap and PTFE connector to the CVAFS carrier gas outlet. Hg isotopes 196, 198, 199, 200, 201, 202, and 204 were monitored for 600 to 1500 seconds. Data was acquired every 0.433 seconds, and integrated (each mass) every 0.02 seconds. Peaks were integrated using Agilent Offline Data Analysis software after visual identification of peak start and end points. Background area was subtracted from peak area. THg was measured by CVAFS alone.

Calibration curves relating counts measured by ICP-MS to mass (ng) measured via CVAFS were developed using dilutions of working standards (0.1, 0.5, 2.5, and 10 ng THg) prepared from a 1000 ppm mercury atomic absorbance standard (Spectrum Chemical Mfg Corp., New Brunswick, NJ).

Linear regressions (Figure S1) were developed to convert ng of total ^{202}Hg or total ^{204}Hg in each sample, measured with CVAFS, to cps of T^{202}Hg and T^{204}Hg , respectively, for input into the kinetic model. The calibration included points at 0.1, 0.5, 2.5, and 10 ng THg. Initial, unspiked T^{202}Hg and T^{204}Hg measured by CVAFS and converted to counts are shown in Table S3 and S4 for all samples modeled to obtain kinetic rate coefficients.

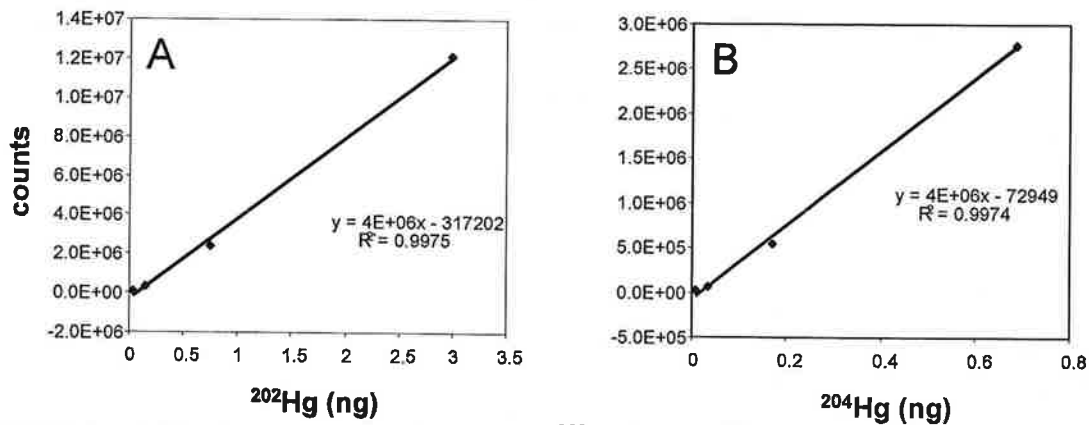


Figure S1. Calibration curves used to convert ^{202}Hg (A) and ^{204}Hg (B) to cps 202 and 204, respectively.

Table S3. Initial, unspiked concentrations of total (THg) and methyl mercury (MeHg) measured in sediment and water for all transects.

Transect		North Summer				
Site		FBN-1	FBN-2	FBN-3	FBN-4	FBN-5
Initial, unspiked concentration	sample type					
THg (ng/L)	water	23.4	12.3	8.43 (0.2 m depth) 8.54 (0.9 m depth)	7.65	9.00
MeHg (ng/L)		9.2	1.47	1.35 (0.2 m depth) 1.83 (0.9 m depth)	0.958	1.64
MeHg/THg (%)		39.3	12.0	16.0 (0.2 m depth) 15.8 (0.9 m depth)	12.5	18.2
THg (ng/g)	sediment	5.30	7.78	14.2	21.8	58.8
MeHg (ng/g)		0.038	0.015	0.067	0.049	0.319
MeHg/THg (%)		0.72	0.19	0.47	0.23	0.54
Transect		North Fall				
Site		FBN-1	FBN-2	FBN-3	FBN-4	
Initial, unspiked concentration	sample type					
THg (ng/L)	water	9.72	7.09	7.65	6.6	
MeHg (ng/L)		0.689	0.615	1.05	0.849	
MeHg/THg (%)		7.1	8.7	13.7	12.9	
THg (ng/g)	sediment	5.85	8.36	6.76	19.1	
MeHg (ng/g)		0.015	0.007	0.020	0.003	
MeHg/THg (%)		0.26	0.08	0.30	0.01	
Transect		South Summer				
Site		FBS-1	FBS-2	FBS-3	FBS-4	FBS-5
Initial, unspiked concentration	sample type					
THg (ng/L)	water	72.2	170	6.26	11.9	47.3
MeHg (ng/L)		1.11	0.193	1.85	0.09	0.233
MeHg/THg (%)		1.54	0.11	29.6	0.76	0.49
THg (ng/g)	sediment	127	204	85.0	73.6	80.0
MeHg (ng/g)		0.217	0.312	0.165	0.032	0.070
MeHg/THg (%)		0.17	0.15	0.19	0.04	0.09
Transect		South Fall				
Site		FBS-1	FBS-2	FBS-3	FBS-4	FBS-5
Initial, unspiked concentration	sample type					
THg (ng/g)	sediment	234	297	17.6	59.4	55.1
MeHg (ng/g)		0.012	0.140	0.103	0.006	0.038
MeHg/THg (%)		0.01	0.05	0.59	0.01	0.07

Kinetic Modeling Input

Table S4.

Mass (counts) for FB sediment initial $T^{202}\text{Hg}$, $T^{204}\text{Hg}$, $M^{202}\text{Hg}$, and $M^{204}\text{Hg}$ (t=0) input into the kinetic model.

Transect	Sample	THg (counts)		MeHg (counts)	
		202	204	202	204
North Summer	FBN-1	7.4E+06	1.35E+07	4914	1158
	FBN-2	8.2E+06	1.36E+07	5711	1298
	FBN-3	1.8E+07	1.60E+07	8678	1967
	FBN-4	2.6E+07	1.77E+07	6641	1551
	FBN-5	7.0E+07	2.78E+07	30946	7065
South Fall	FBS-1	2.81E+08	2.49E+08	1648	412
	FBS-2	3.92E+08	2.74E+08	20242	4722
	FBS-3	2.46E+07	1.90E+08	13452	3075
	FBS-4	7.24E+07	2.01E+08	926	225
	FBS-5	7.39E+07	2.01E+08	4830	1242
North Fall	FBN-1	7.45E+06	8.78E+06	10900	2503
	FBN-2	1.08E+07	9.54E+06	4332	1002
	FBN-3	7.83E+06	8.87E+06	13086	3080
	FBN-4	2.49E+07	1.28E+07	2038	503

Masses (counts) for OB sediment initial $T^{202}\text{Hg}$, $T^{204}\text{Hg}$, $M^{202}\text{Hg}$, and $M^{204}\text{Hg}$ (t=0) input into the kinetic model.

Site	$T^{202}\text{Hg}$	$T^{204}\text{Hg}$	$M^{202}\text{Hg}$	$M^{204}\text{Hg}$
	counts		counts	
OB-1	36614617	15581067	301845	68579
OB-2	15222848	10319909	345412	77543
OB-3	41916850	16885115	314261	71102
OB-4	27290000	13287742	529039	121887
OB-5	22079184	12006178	98428	23693

Kinetic Modeling Sensitivity Analysis

Figure S2 shows sensitivity of model fit in response to k_{meth} ranging over two orders of magnitude ($1.0E-6$ to $1.0E-4$ hr^{-1} , with k_{BA} set equal to $1.0E-2$ hr^{-1}) for the north transect (summer) sediment samples from site FBN-1. The range of rate constant values used to generate the model results in Figure S2 was previously narrowed from a larger range, by determining the subset range over which RSS values were minimized. At the lower value of k_{meth} (Figure S2, top), the model fails to represent the observed temporal trends in $R_{MeHg}(t)$ and $[M^{202}Hg](t)$ and $[M^{204}Hg](t)$. Notably, all other values of k_{meth} yielded reasonable representations of $R_{MeHg}(t)$ (Figure S2, left), but in some cases yielded very poor representations of $[MeHg](t)$ (Figure S2, right), thereby necessitating the use of counts as an additional matching constraint. At the upper value of k_{meth} , the modeled $[M^{202}Hg]$ and $[M^{204}Hg]$ pg greatly over-predict the measured pg (Figure S2, bottom). The combined criteria yielded a range of acceptable values for k_{meth} from $3.0E-5$ to $7.0E-5$, and for k_{demeth} from $5.0E-3$ to $2.0E-2$ (for site FBN-1 summer), with best-fit values being $k_{meth} = 5.0E-5$ hr^{-1} and $k_{demeth} = 1.25E-2$ hr^{-1} . The best-fit values were the median of the range between the operational upper and lower limits (described in Methods), which were used to define error bars in the corresponding figures. This process was performed for all sites.

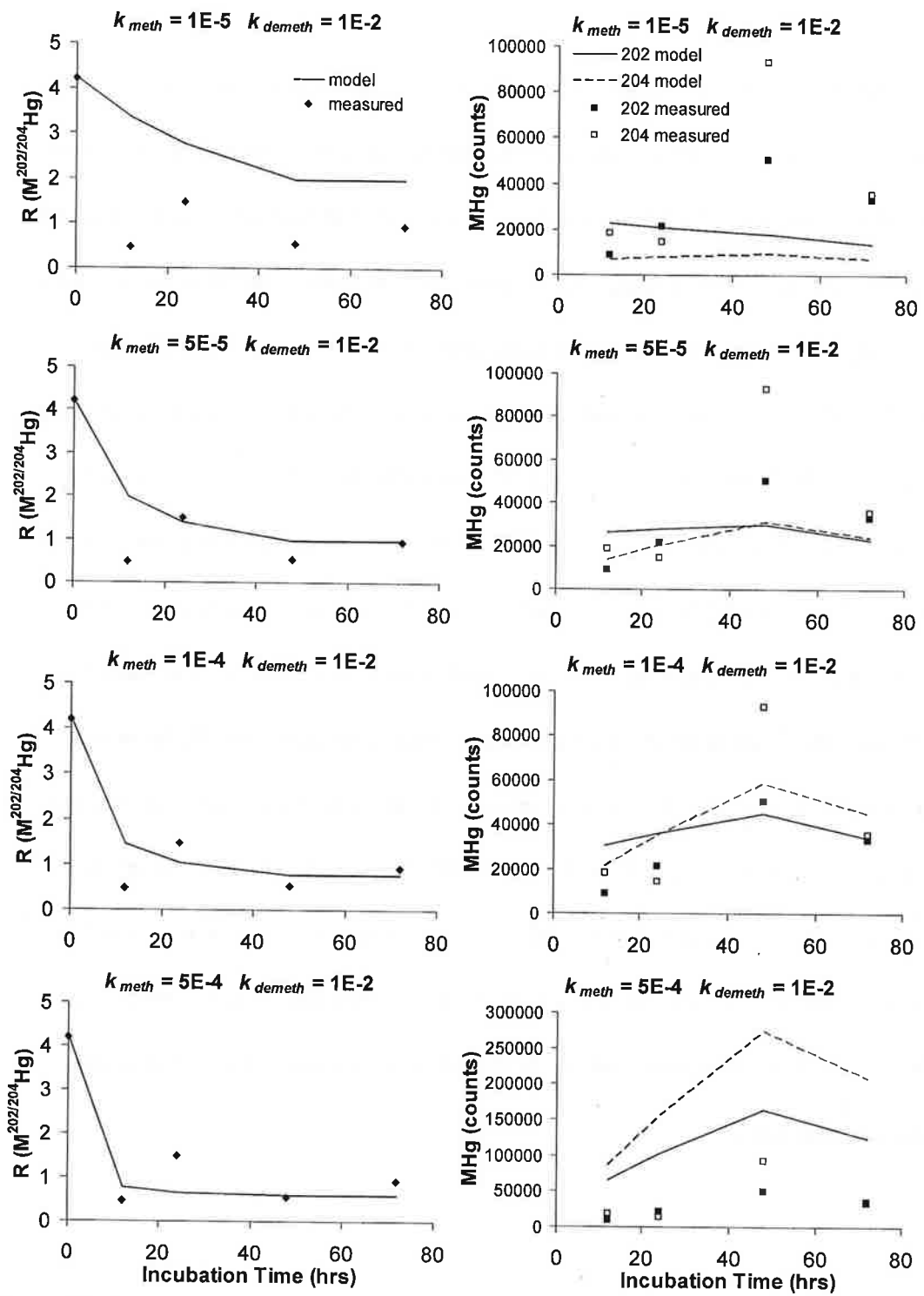


Figure S2. Sensitivity of model fit to measured data. Measured data (symbols) for $R_{MeHg}(t)$, $[M^{202}Hg](t)$ and $[M^{204}Hg](t)$ for the north summer transect site FBN-1 and

modeled values (lines) for $k_{BA} = 0.01$. Initial values for $[M^{202}\text{Hg}](t)$ and $[M^{204}\text{Hg}](t)$ are given in Table S4.

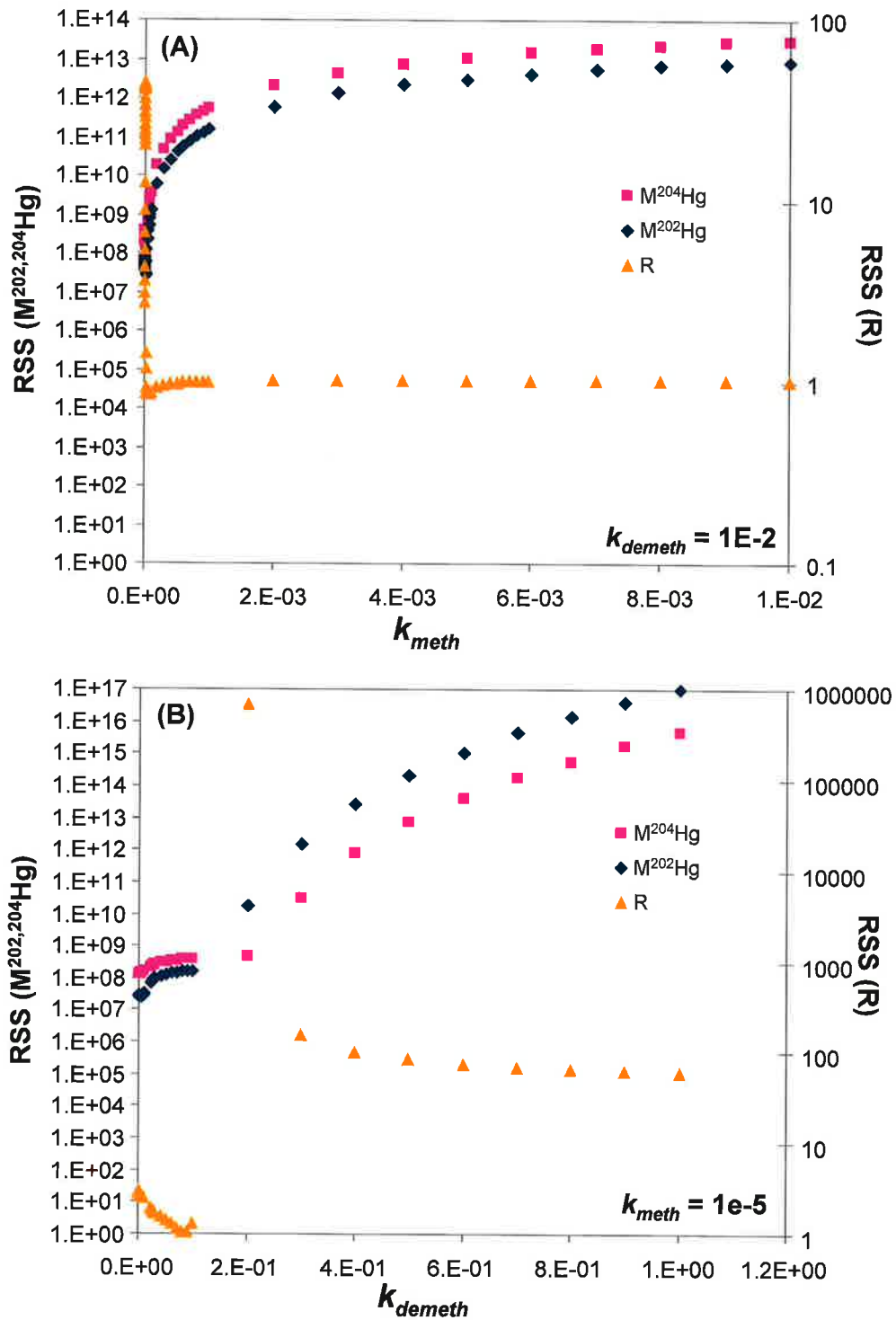


Figure S3. RSS curves for FBN-1 summer with $k_{demeth} = 1E-2$ (A) and $k_{meth} = 1E-5$ (B).

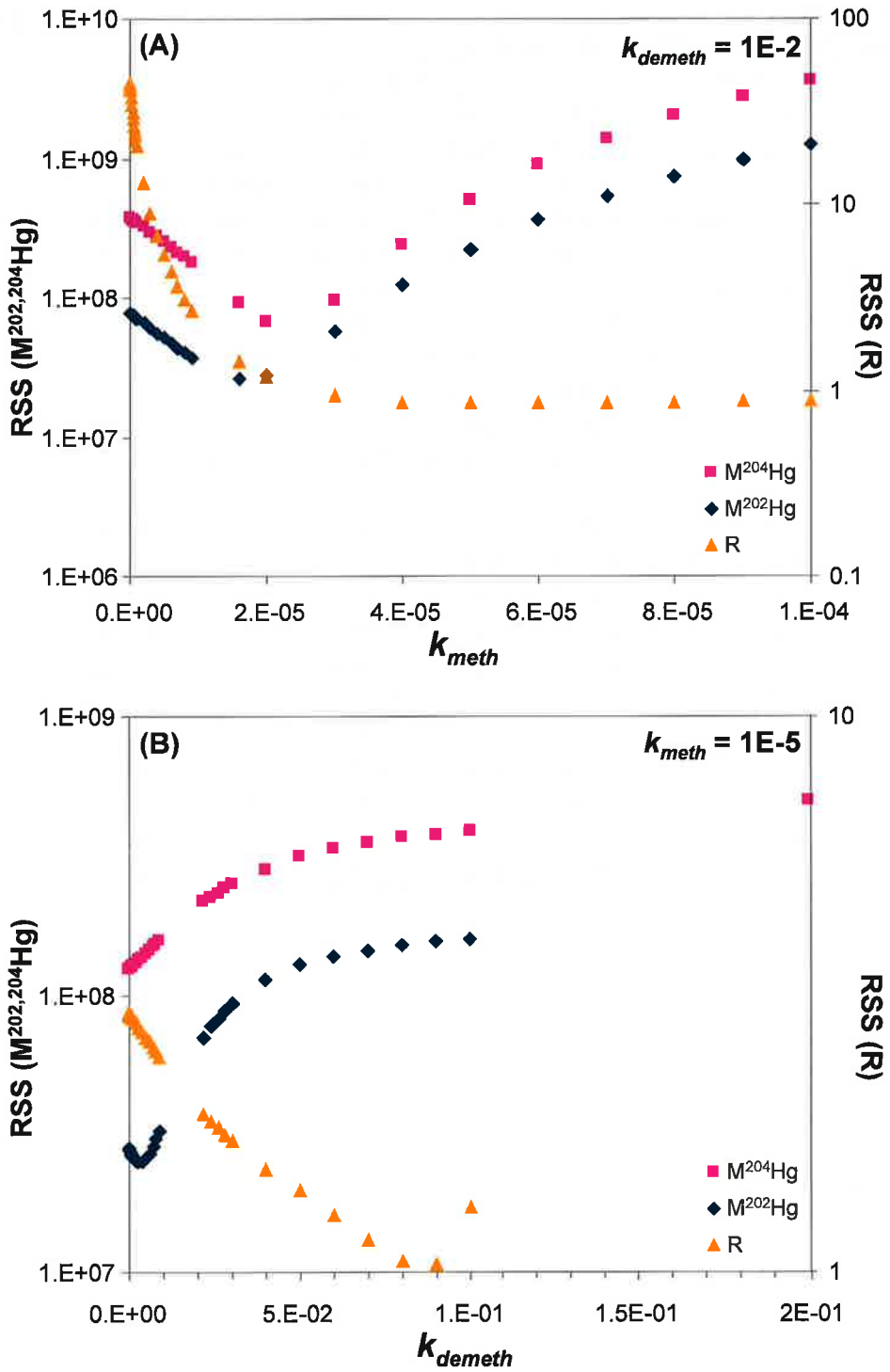


Figure S4. RSS curves for FBN-1 summer with $k_{BA} = 1E-2$ and $k_{AB} = 1E-5$. (Same plots from Figures S2(A and B) with zoomed in scale.)

Table S5. Best-fit kinetic rate constants k_{meth} and k_{demeth} resulting from modeling of sediment $[M^{202}Hg](t)$, $[M^{204}Hg](t)$ and $R(t)_{MeHg}$.

Transect	FBN Summer				
Site	FBN-1	FBN-2	FBN-3	FBN-4	FBN-5
k_{meth} (hrs ⁻¹)	2.1E-04	3.8E-05	6.0E-06	1.3E-04	7.0E-06
±	3.0E-05	6.0E-06	4.0E-06	2.5E-05	5.0E-06
k_{demeth} (hrs ⁻¹)	1.2E-02	4.0E-03	5.0E-04	1.2E-02	3.4E-03
±	2.5E-03	3.0E-03	5.0E-04	3.5E-03	2.6E-03
Transect	FBN Fall				
Site	FBN-1	FBN-2	FBN-3	FBN-4	
k_{meth} (hrs ⁻¹)	1.1E-03	7.5E-05	1.7E-04	1.4E-06	
±	1.5E-04	2.5E-05	3.5E-05	6.0E-07	
k_{demeth} (hrs ⁻¹)	1.5E-02	5.0E-03	5.0E-03	5.0E-04	
±	5.0E-03	2.5E-03	2.5E-03	7.5E-04	
Transect	FBS Fall				
Site	FBS-1	FBS-2	FBS-3	FBS-4	FBS-5
k_{meth} (hrs ⁻¹)	8.1E-07	8.0E-07	1.1E-05	2.8E-06	1.3E-06
±	3.9E-07	2.0E-07	3.8E-06	1.3E-06	7.0E-07
k_{demeth} (hrs ⁻¹)	5.0E-05	5.0E-06	2.5E-05	5.0E-06	5.0E-05
±	5.0E-05	5.0E-06	2.5E-05	5.0E-06	5.0E-05
Transect	OB Summer				
Site	OB-1	OB-2	OB-3	OB-4	OB-5
k_{meth} (hrs ⁻¹)	1.3E-04	5.4E-04	2.7E-04	5.0E-04	2.8E-04
±	7.5E-05	2.8E-04	6.4E-05	2.0E-04	7.0E-05
k_{demeth} (hrs ⁻¹)	2.5E-03	1.2E-02	3.2E-02	2.9E-02	2.3E-02
±	1.5E-03	4.5E-03	2.0E-03	1.0E-03	3.0E-03

Table S6. Best-fit kinetic rate constants k_{meth} and k_{demeth} converted from Table S6 values to $\text{ng}\cdot\text{g}^{-1}\cdot\text{day}^{-1}$ (dry weight).

Transect	FBN summer				
Site	FBN-1	FBN-2	FBN-3	FBN-4	FBN-5
k_{meth} ($\text{ng g}^{-1} \text{d}^{-1}$)	1.8E-03	1.0E-04	4.4E-05	1.4E-03	2.5E-04
±	2.6E-04	1.6E-05	3.0E-05	2.8E-04	1.8E-04
k_{demeth} ($\text{ng g}^{-1} \text{d}^{-1}$)	9.8E-02	1.1E-02	3.7E-03	1.3E-01	1.2E-01
±	2.1E-02	7.9E-03	3.7E-03	3.9E-02	9.2E-02
Transect	FBN fall				
Site	FBN-1	FBN-2	FBN-3	FBN-4	
k_{meth} ($\text{ng g}^{-1} \text{d}^{-1}$)	5.6E-03	1.1E-04	7.3E-04	1.0E-06	
±	8.1E-04	3.7E-05	1.5E-04	4.3E-07	
k_{demeth} ($\text{ng g}^{-1} \text{d}^{-1}$)	8.1E-02	7.4E-03	2.2E-02	3.6E-04	
±	2.7E-02	3.7E-03	1.1E-02	5.4E-04	
Transect	FBS fall				
Site	FBN-1	FBN-2	FBN-3	FBN-4	FBN-5
k_{meth} ($\text{ng g}^{-1} \text{d}^{-1}$)	1.4E-06	2.1E-05	5.1E-05	2.0E-06	5.2E-06
±	6.7E-07	5.2E-06	1.7E-05	9.1E-07	2.8E-06
k_{demeth} ($\text{ng g}^{-1} \text{d}^{-1}$)	8.6E-05	1.3E-04	1.1E-04	3.6E-06	2.0E-04
±	8.6E-05	1.3E-04	1.1E-04	3.6E-06	2.0E-04
Transect	OB summer				
Site	FBN-1	FBN-2	FBN-3	FBN-4	FBN-5
k_{meth} ($\text{ng g}^{-1} \text{d}^{-1}$)	5.5E-03	1.7E-02	2.4E-03	2.6E-02	2.2E-03
±	3.3E-03	8.7E-03	5.7E-04	1.0E-02	5.4E-04
k_{demeth} ($\text{ng g}^{-1} \text{d}^{-1}$)	1.1E-01	3.7E-01	2.8E-01	1.5E+00	1.8E-01
±	6.7E-02	1.4E-01	1.8E-02	5.1E-02	2.3E-02

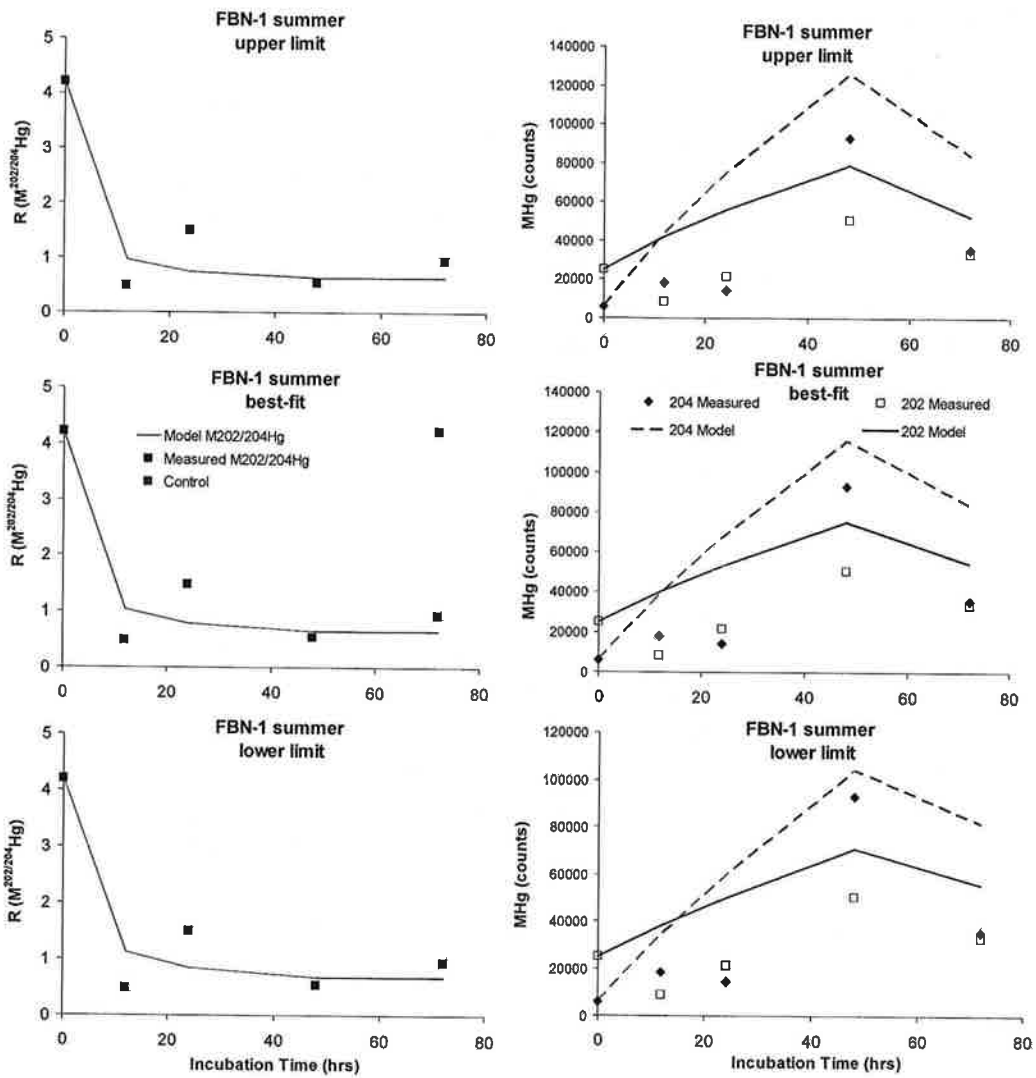


Figure S5. Best-fit, lower limit, and upper limit model fits for FBN-1 summer.

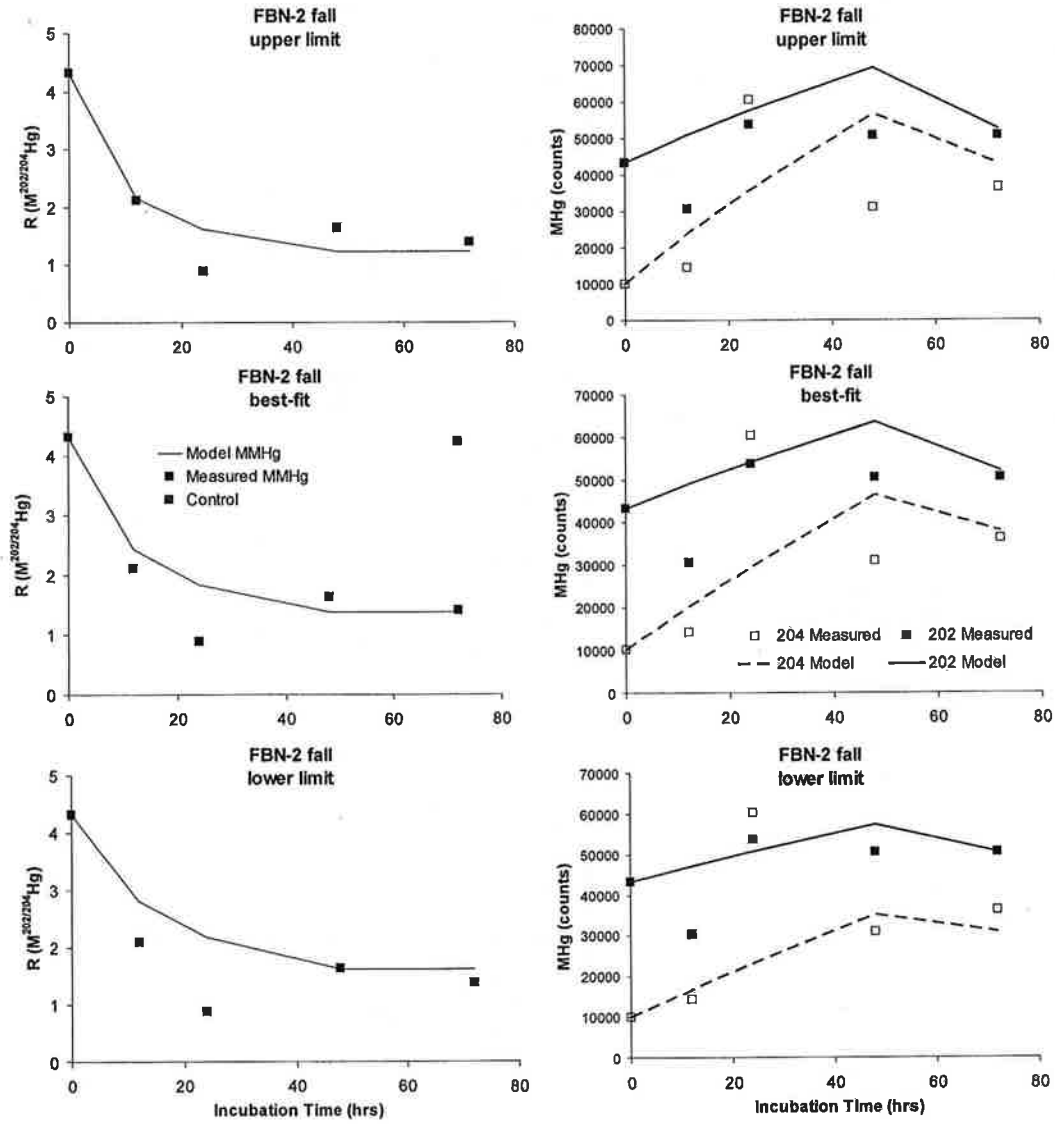


Figure S6. Best-fit, lower limit, and upper limit model fits for FBN-2 fall.

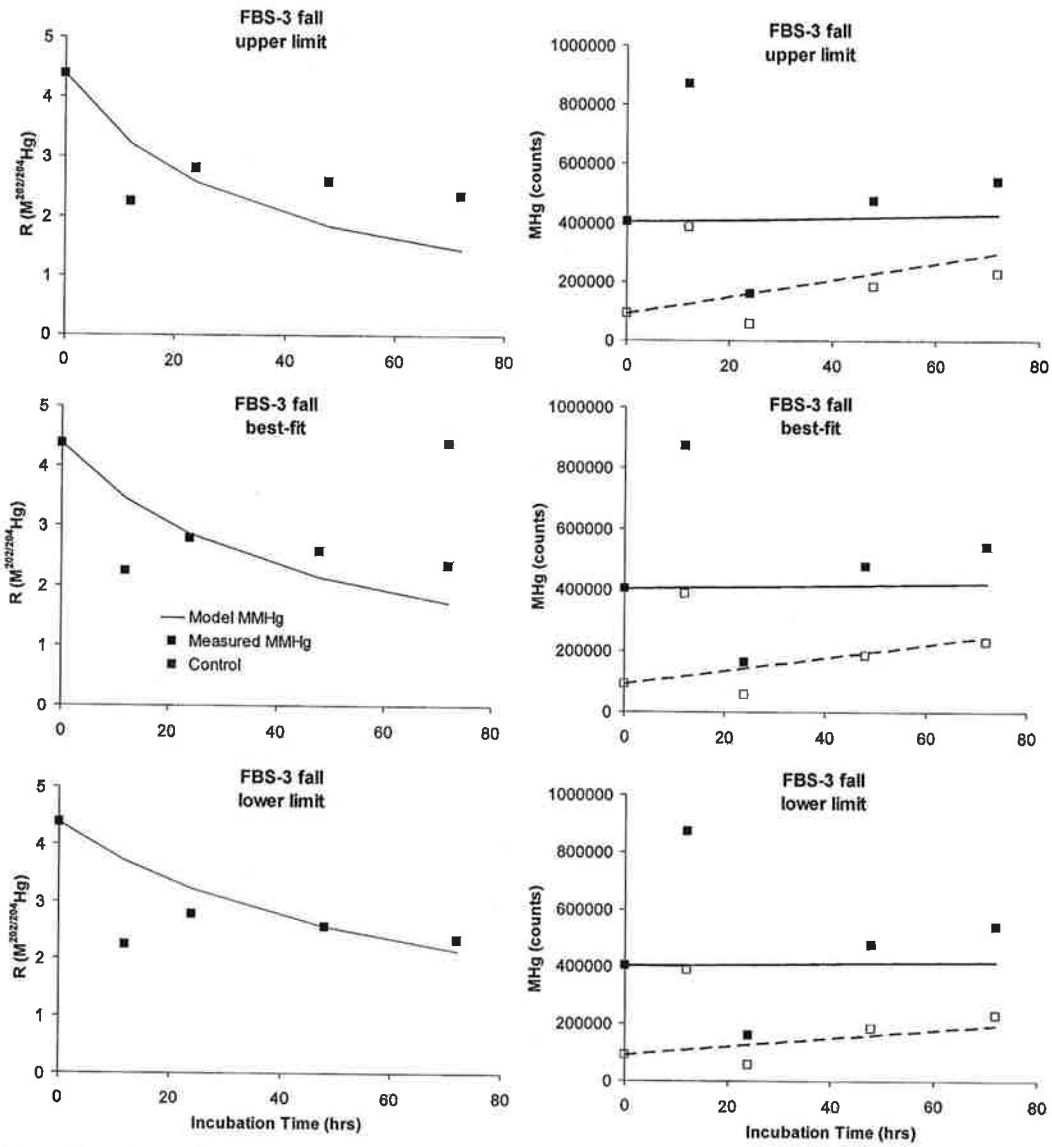


Figure S7. Best-fit, lower limit, and upper limit model fits for FBS-3 fall.

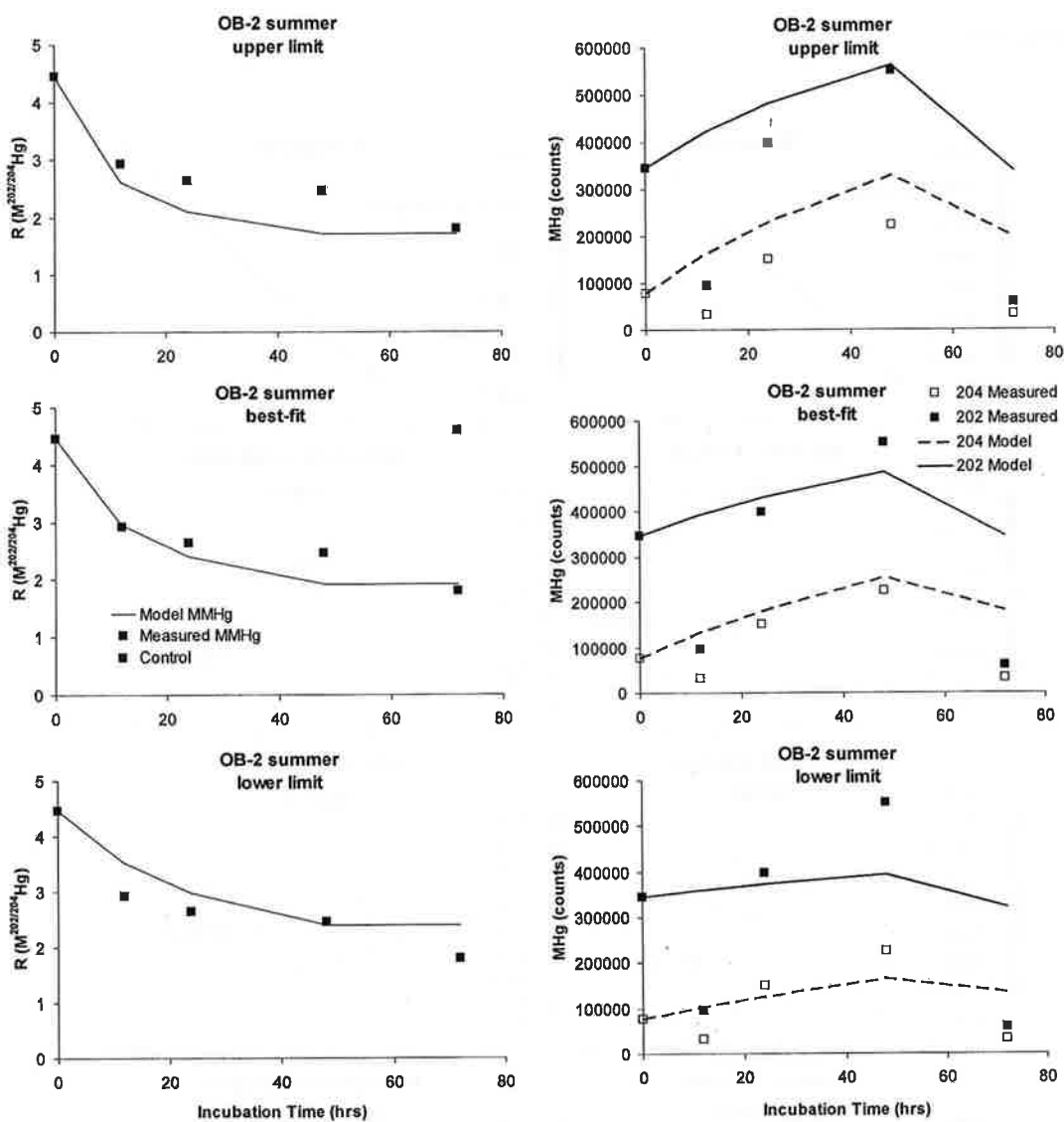


Figure S8. Best-fit, lower limit, and upper limit model fits for OB-2 summer.

Correlations

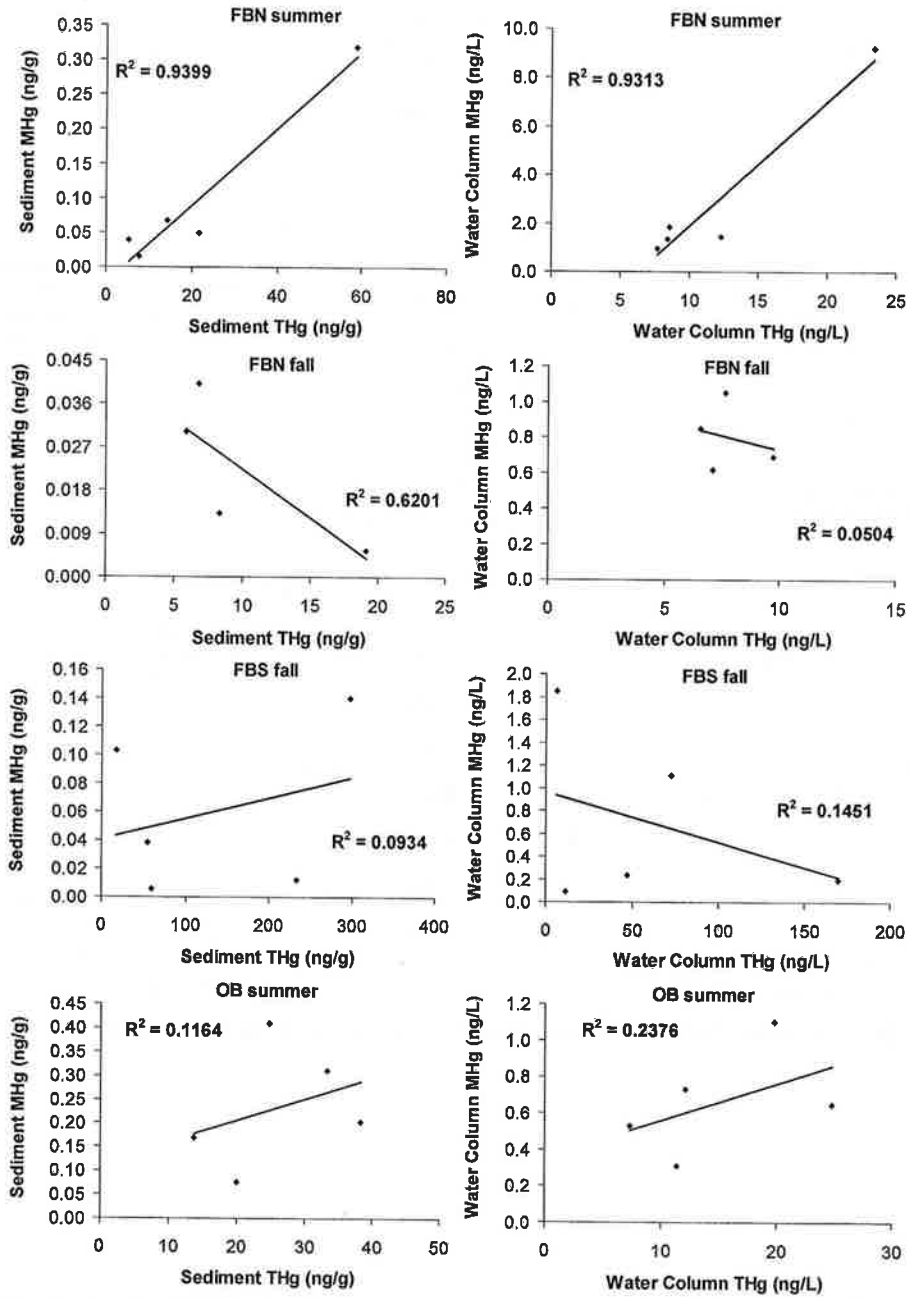


Figure S9. Linear correlations of sediment and water column THg and MeHg for all transects.

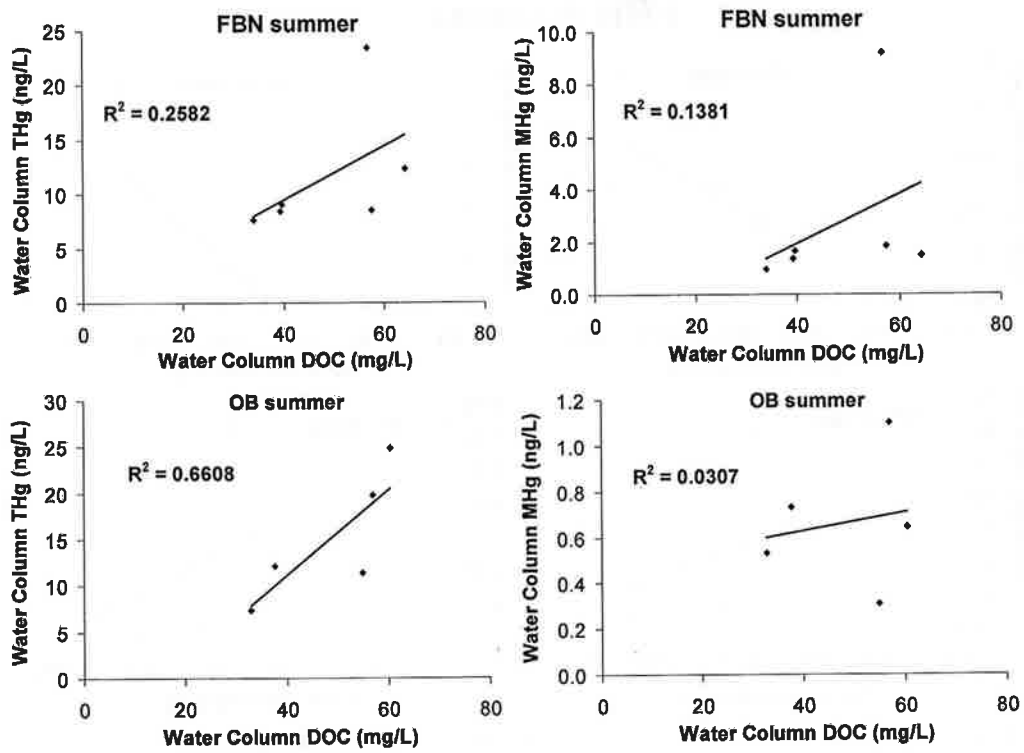


Figure S10. Linear correlations of water column THg and MeHg and water column DOC for FBN summer and OB summer transects.

FBN summer

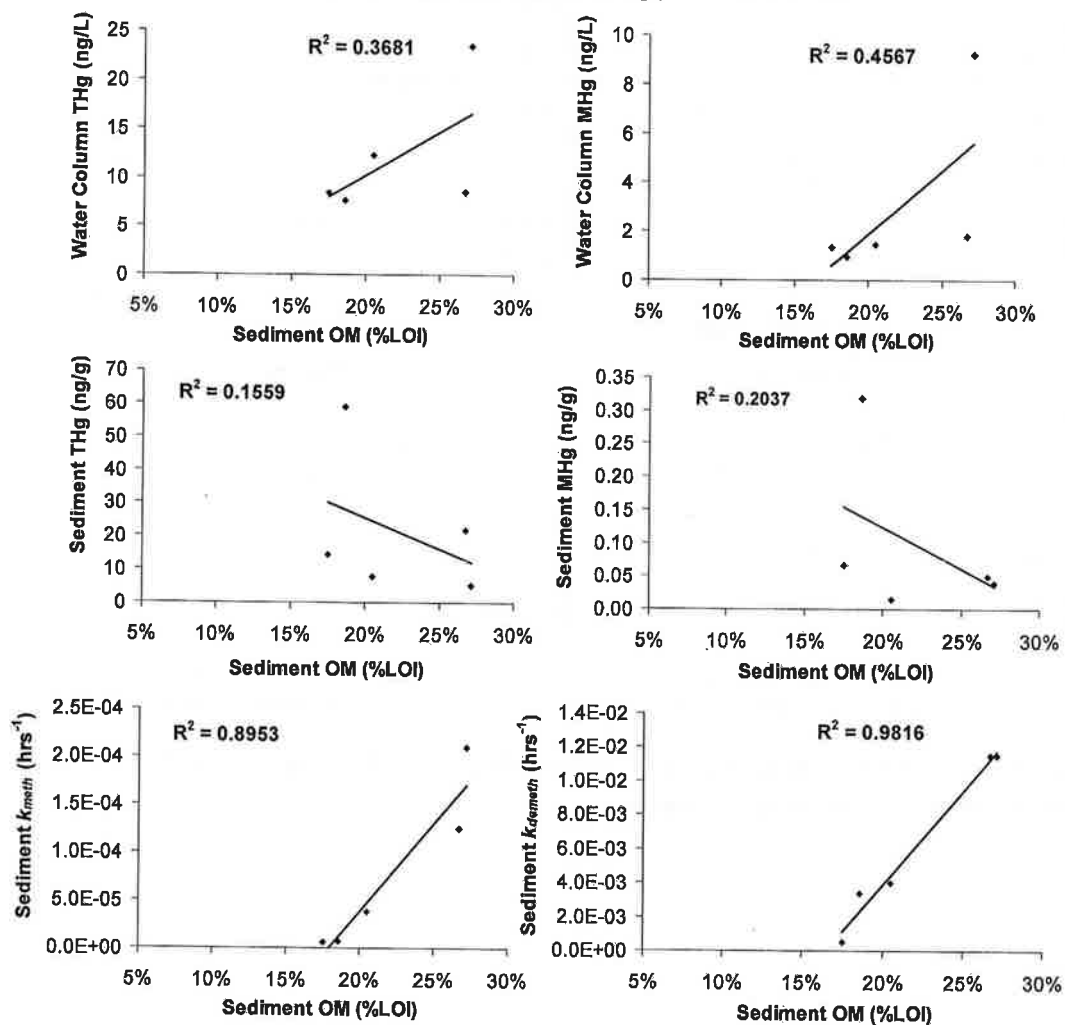


Figure S11. Linear correlations of sediment and water column THg and MeHg and sediment k_{meth} and k_{demeth} versus sediment organic matter (%LOI) for FBN summer.

FBN fall

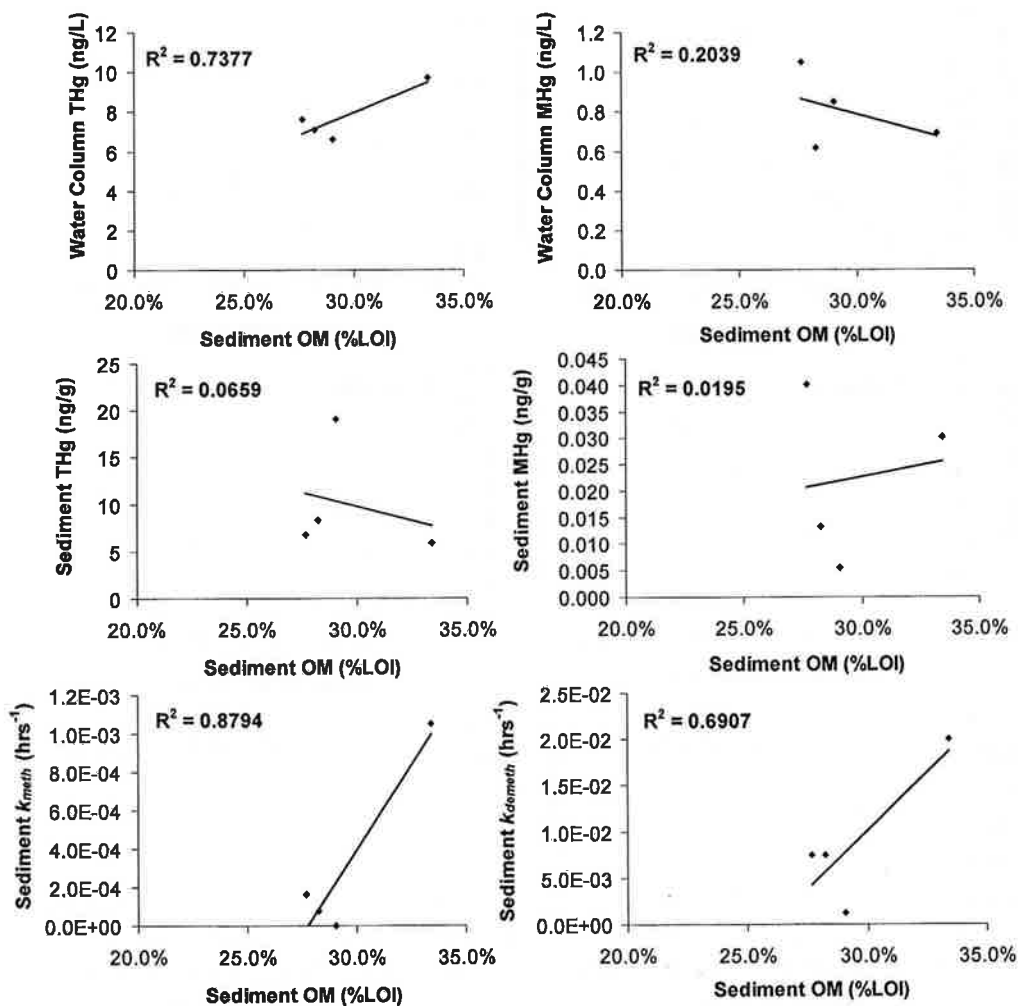


Figure S12. Linear correlations of sediment and water column THg and MeHg and sediment k_{meth} and k_{demeth} versus sediment organic matter (%LOI) for FBN fall.

FBS fall

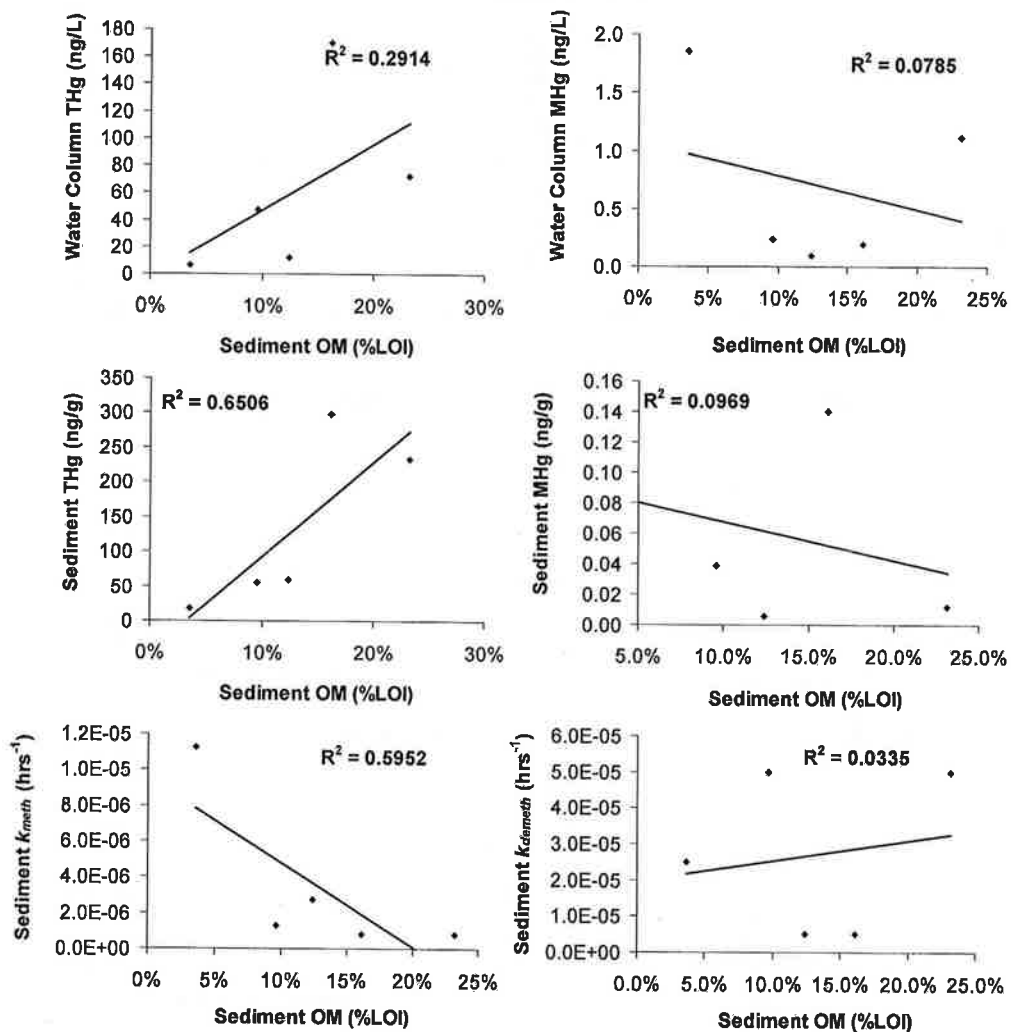


Figure S13. Linear correlations of sediment and water column THg and MeHg and sediment k_{meth} and k_{demeth} versus sediment organic matter (%LOI) for FBS fall.

OB summer

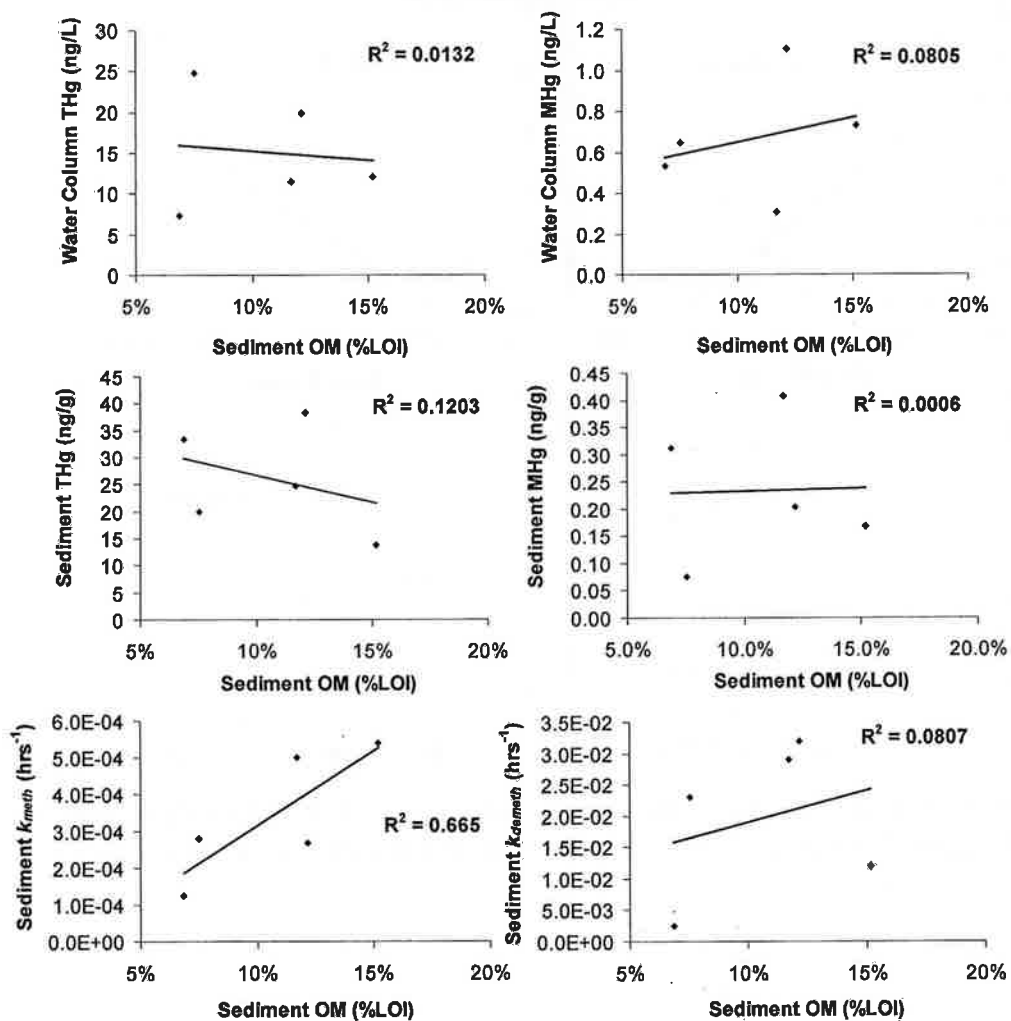


Figure S14. Linear correlations of sediment and water column THg and MeHg and sediment k_{meth} and k_{demeth} versus sediment organic matter (%LOI) for OB summer.

FBN summer

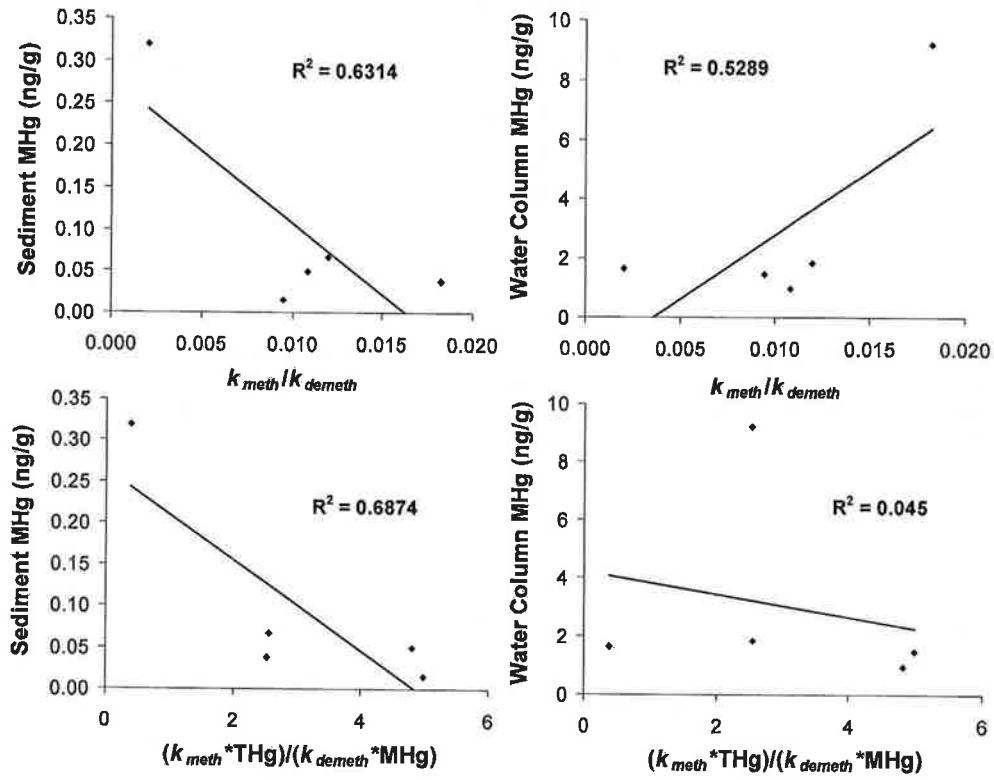


Figure S15. Linear correlations of sediment and water column THg and MeHg and ratios of k_{meth}/k_{demeth} (top) and $(k_{meth} * THg) / (k_{demeth} * MTHg)$ for transect FBN summer.

FBN fall

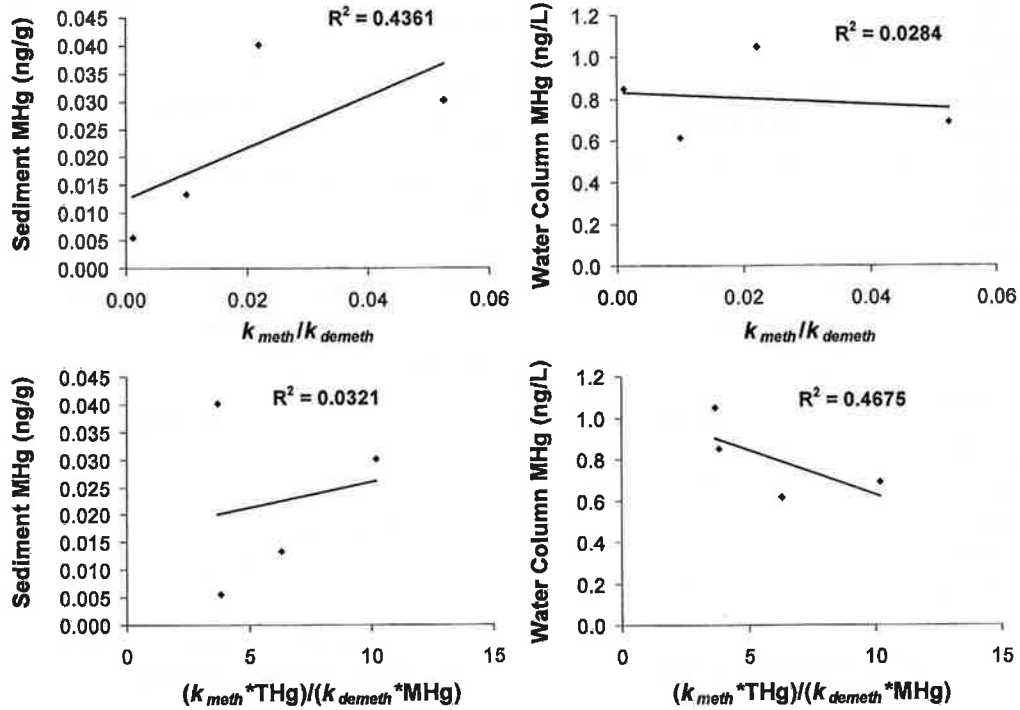


Figure S16. Linear correlations of sediment and water column THg and MeHg and ratios of k_{meth}/k_{demeth} (top) and $(k_{meth} * THg) / (k_{demeth} * MeHg)$ for transect FBN fall.

FBS fall

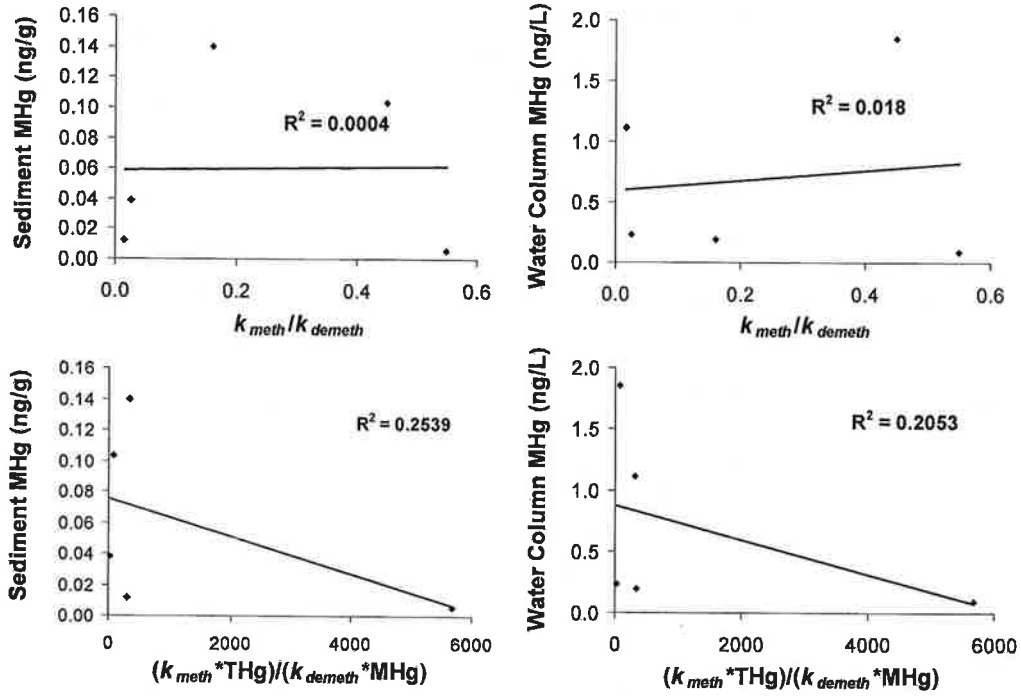


Figure S17. Linear correlations of sediment and water column THg and MeHg and ratios of k_{meth}/k_{demeth} (top) and $(k_{meth} * THg)/(k_{demeth} * MeHg)$ for transect FBS fall.

OB summer

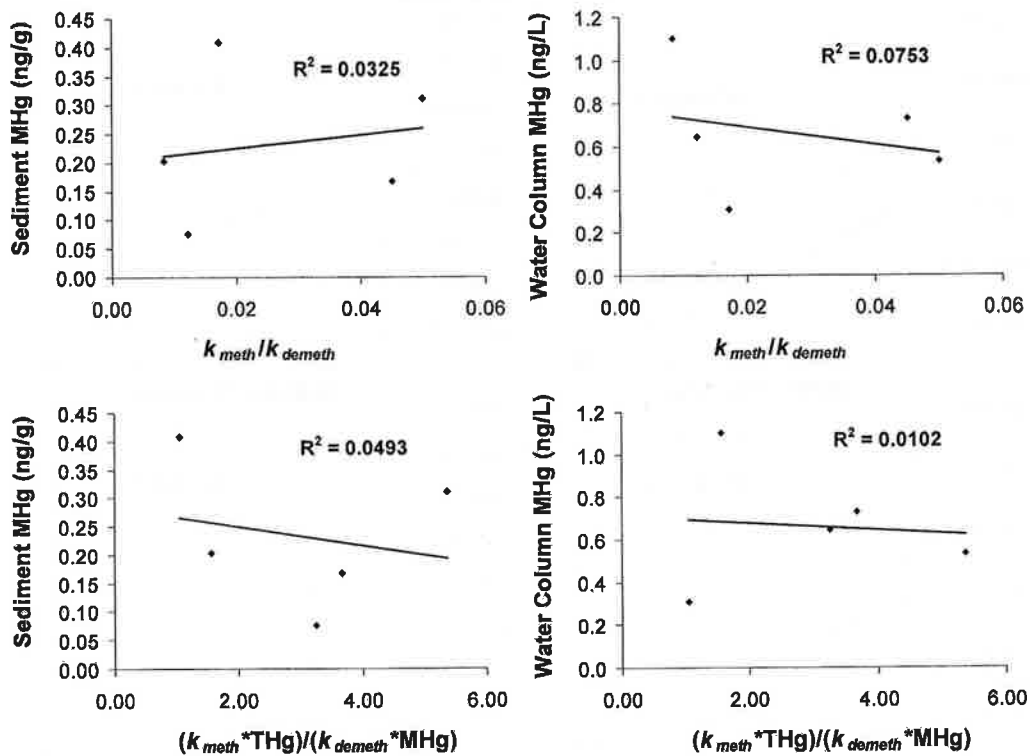


Figure S18. Linear correlations of sediment and water column THg and MeHg and ratios of k_{meth}/k_{demeth} (top) and $(k_{meth} * THg)/(k_{demeth} * MeHg)$ for transect OB summer.

FBN summer

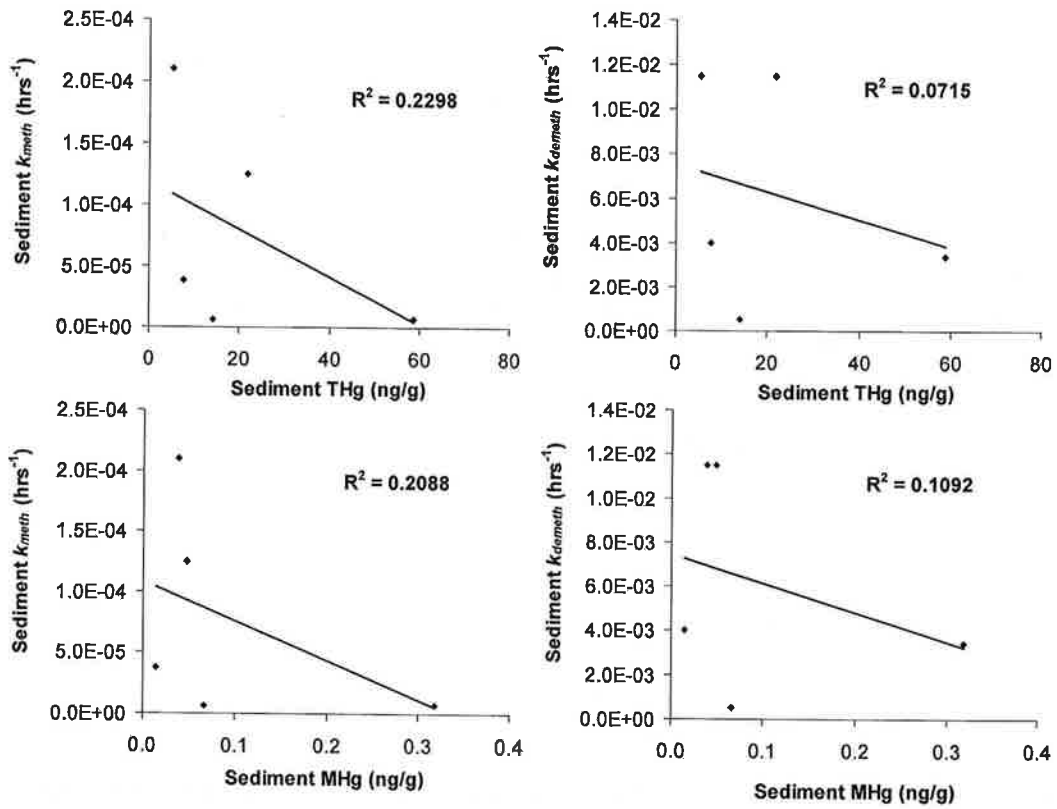


Figure S19. Linear correlations of sediment THg and MeHg and sediment k_{meth} and k_{demeth} for FBN summer.

FBN fall

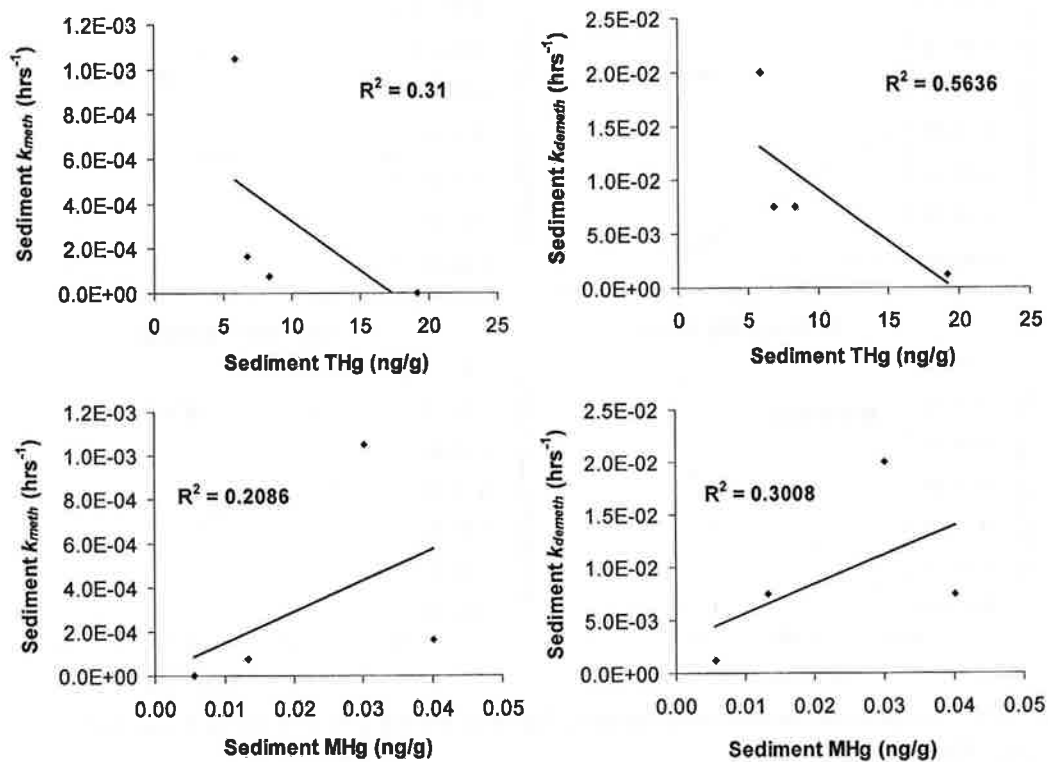


Figure S20. Linear correlations of sediment THg and MeHg and sediment k_{meth} and k_{demeth} for FBN fall.

FBS fall

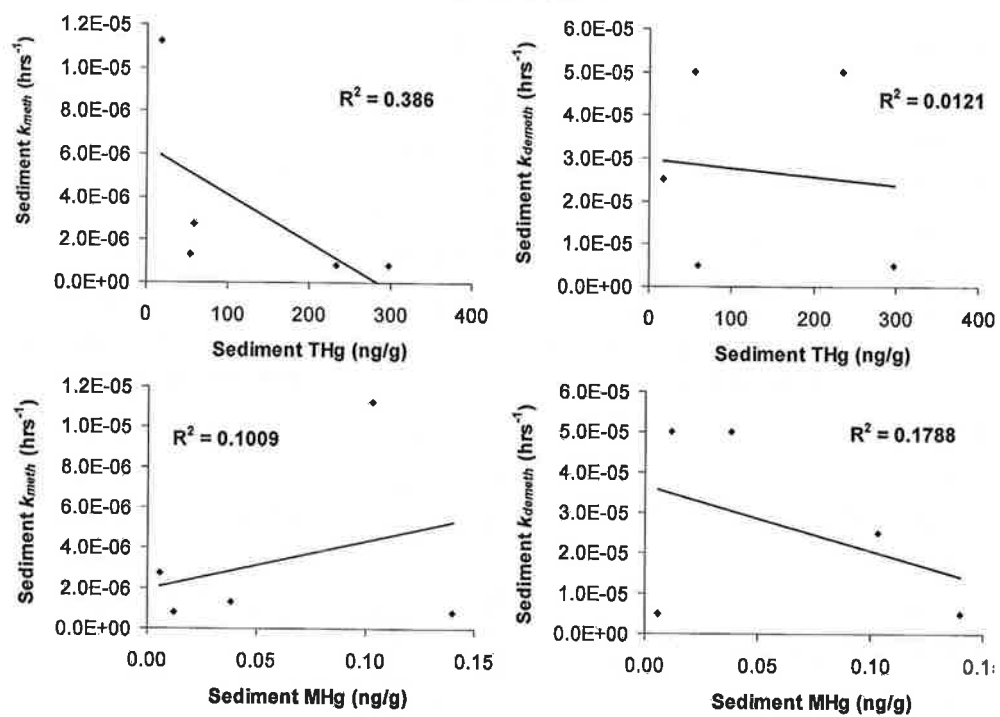


Figure S21. Linear correlations of sediment THg and MeHg and sediment k_{meth} and k_{demeth} for FBS fall.

OB summer

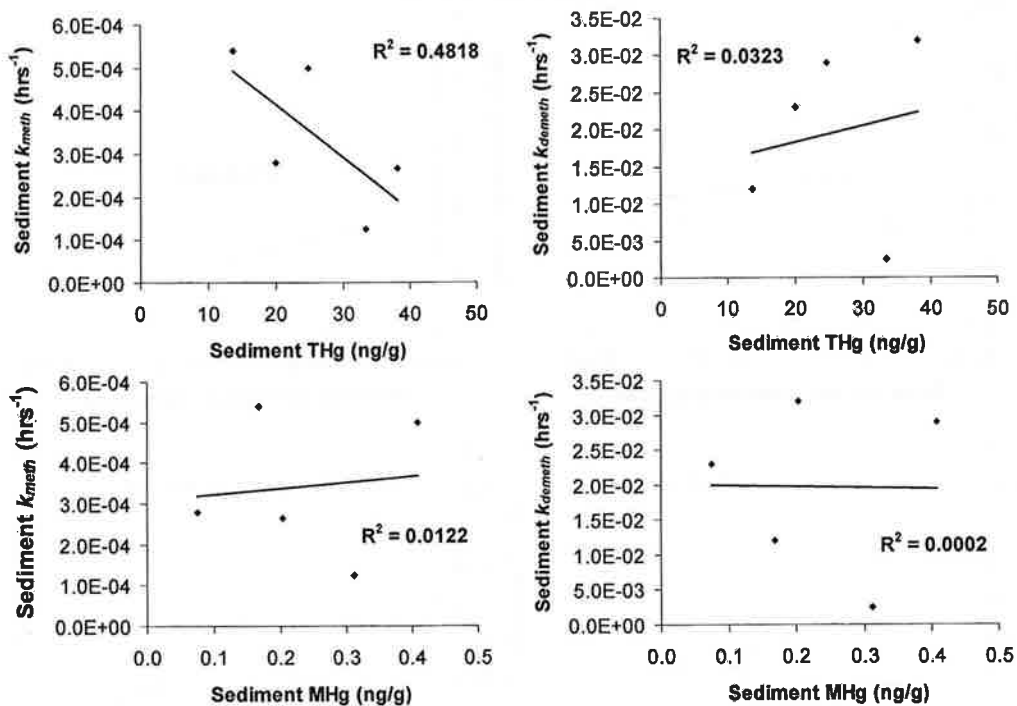


Figure S22. Linear correlations of sediment THg and MeHg and sediment k_{meth} and k_{demeth} for OB summer.

FBN summer

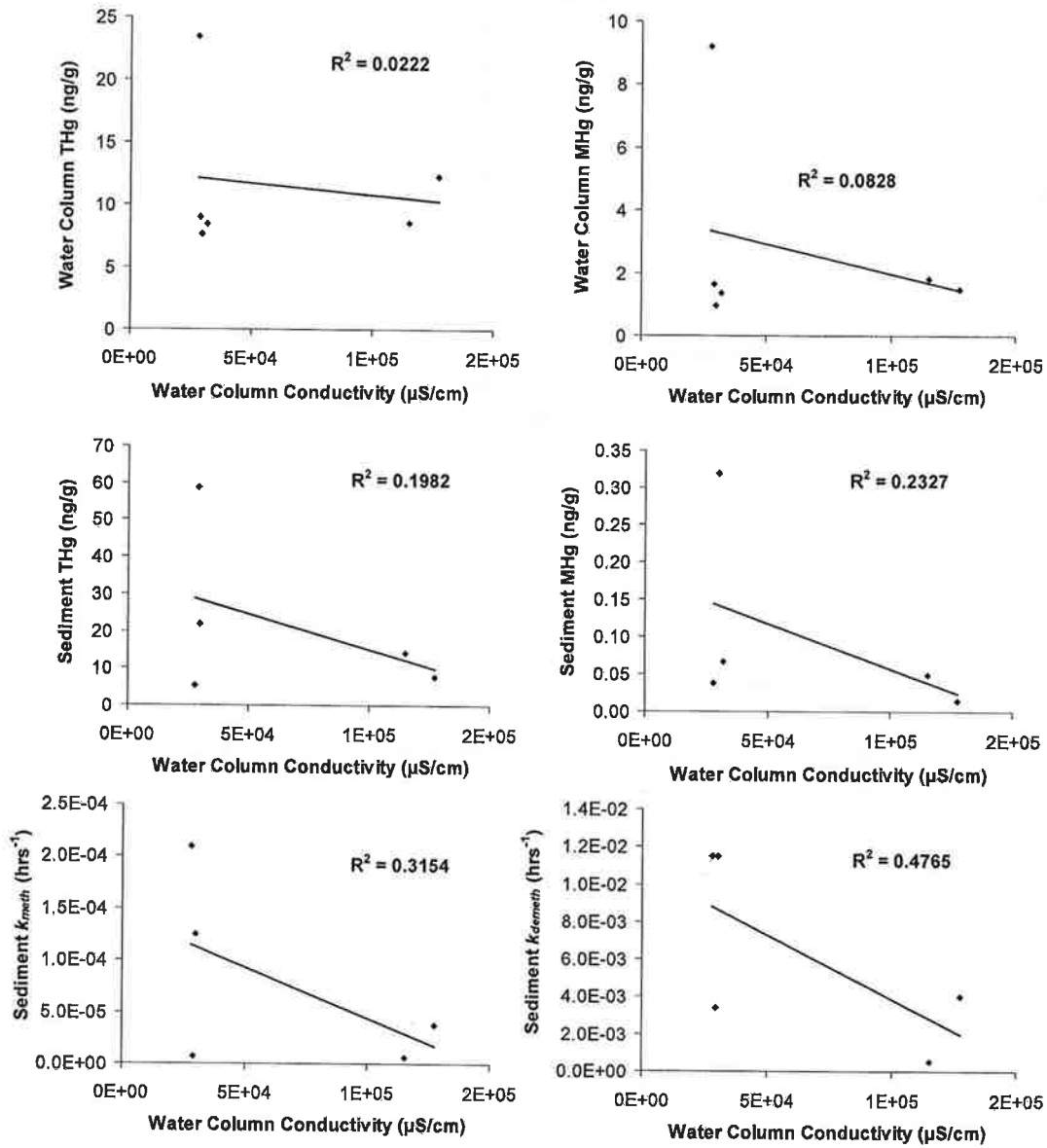


Figure S23. Linear correlations of sediment and water column THg and MeHg and sediment k_{meth} and k_{demeth} versus water column conductivity for FBN summer.

FBN fall

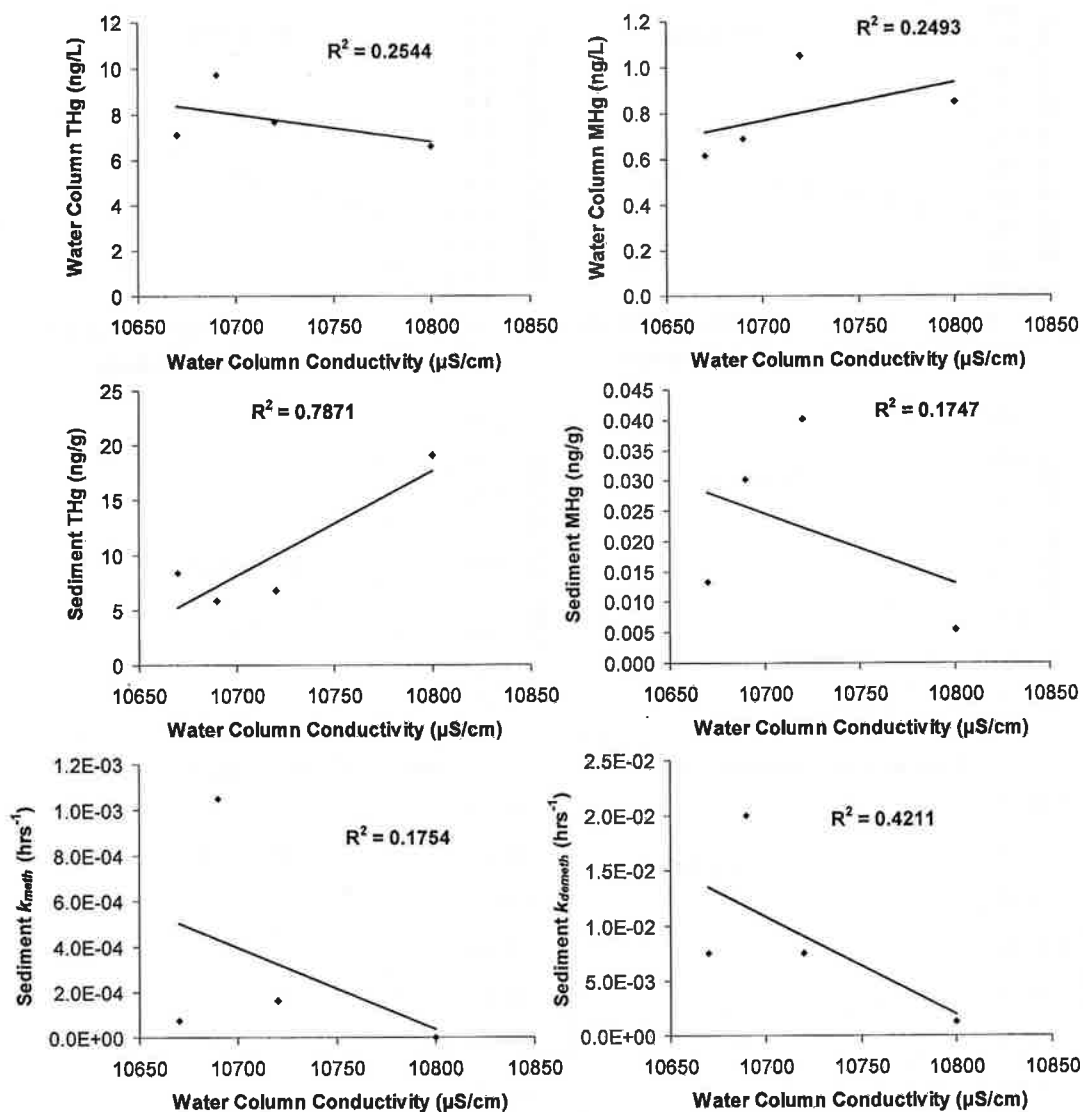


Figure S24. Linear correlations of sediment and water column THg and MeHg and sediment k_{meth} and k_{demeth} versus water column conductivity for FBN fall.

FBS fall

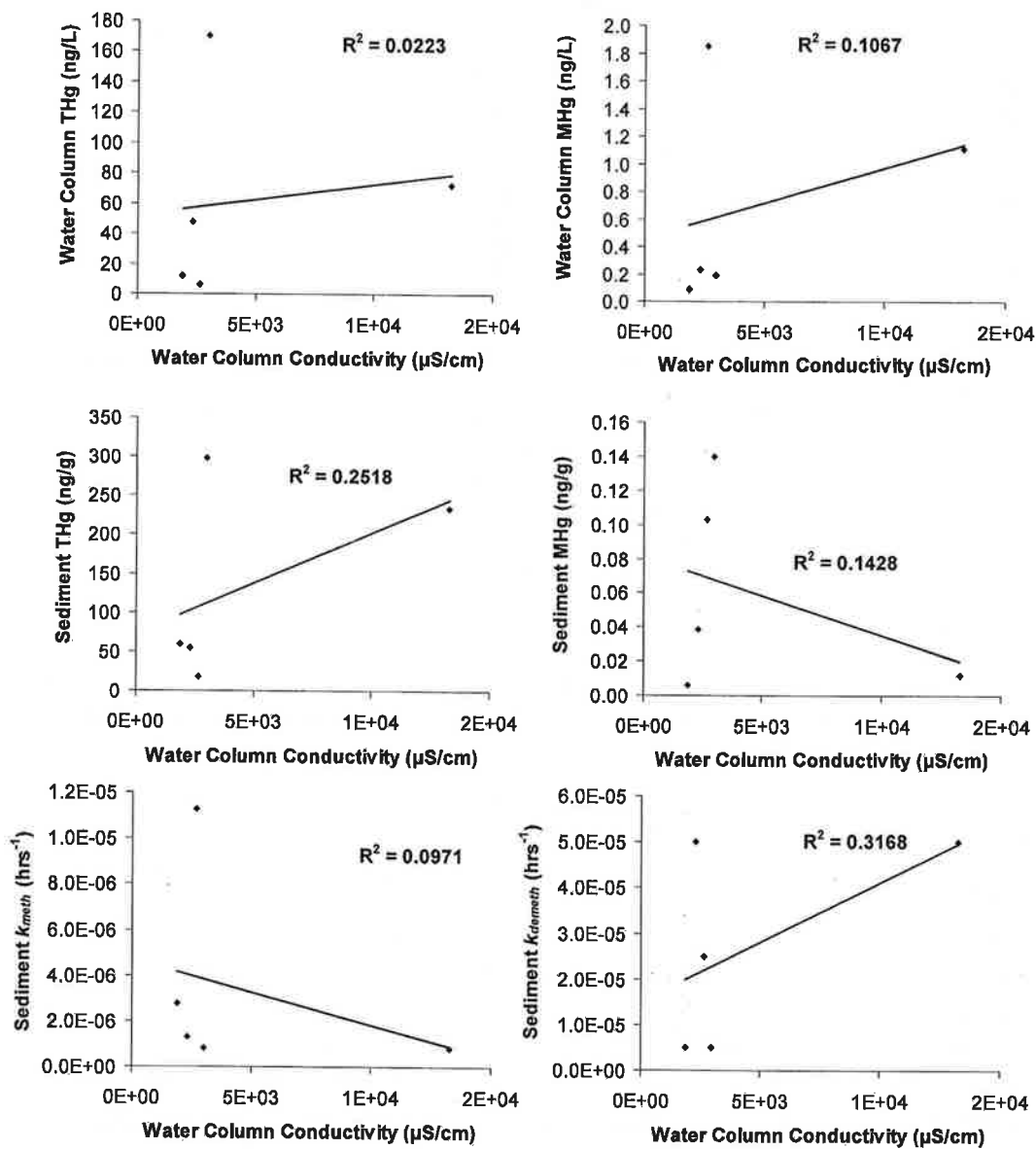


Figure S25. Linear correlations of sediment and water column THg and MeHg and sediment k_{meth} and k_{demeth} versus water column conductivity for FBS fall.

OB summer

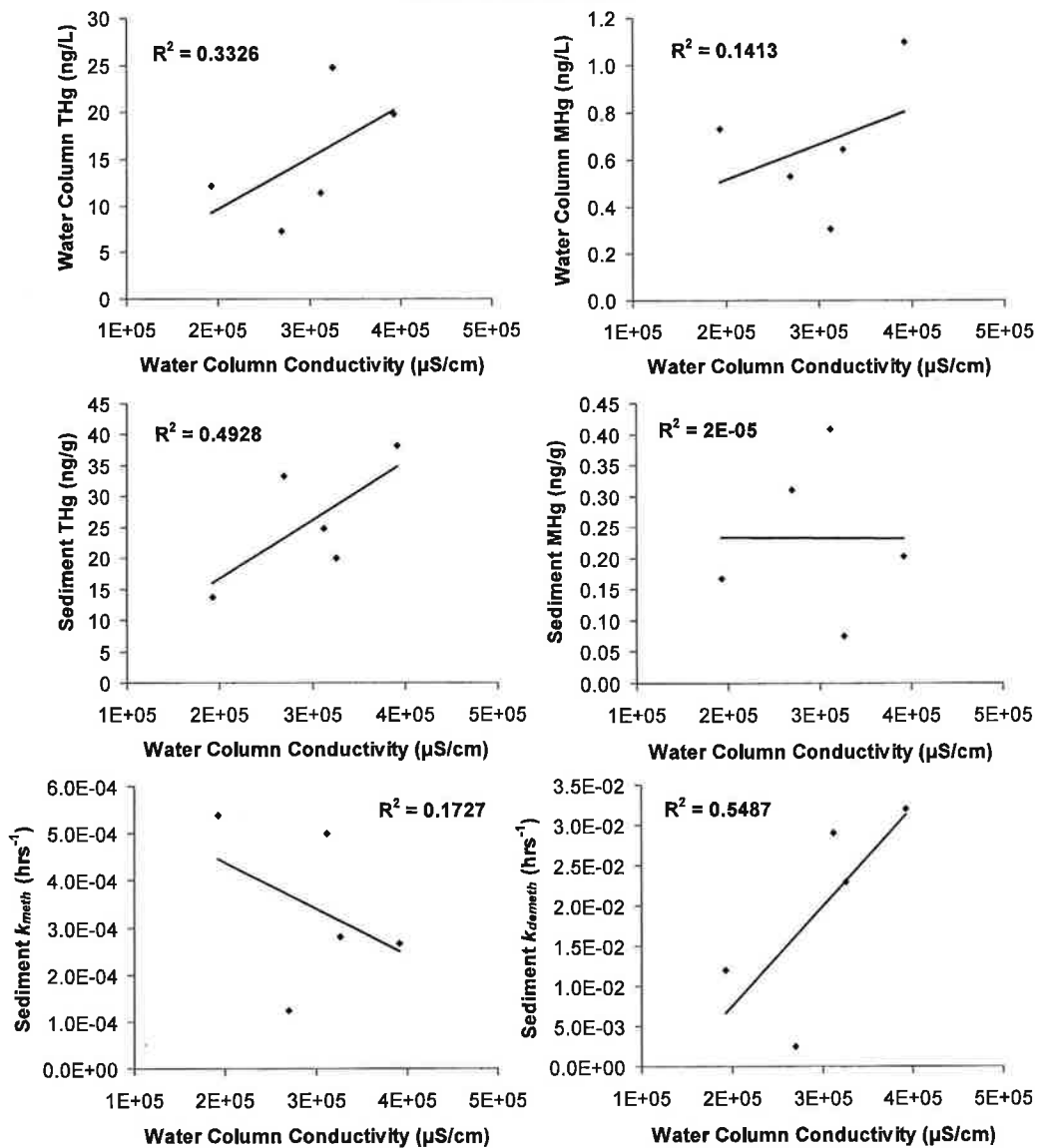


Figure S26. Linear correlations of sediment and water column THg and MeHg and sediment k_{meth} and k_{demeth} versus water column conductivity for OB summer.